

Portland State University

PDXScholar

Geology Faculty Publications and Presentations

Geology

2021

Toward an Integrative Geological and Geophysical View of Cascadia Subduction Zone Earthquakes

Maureen A.L. Walton

US Geological Survey, Santa Cruz

Lydia M. Staisch

US Geological Survey, Portland

Tina Dura

Virginia Tech

Jessie K. Pearl

US Geological Survey, Seattle

Brian Sherrod

US Geological Survey, Seattle

See next page for additional authors

Follow this and additional works at: https://pdxscholar.library.pdx.edu/geology_fac



Part of the [Geology Commons](#)

Let us know how access to this document benefits you.

Citation Details

Walton, M. A., Staisch, L. M., Dura, T., Pearl, J. K., Sherrod, B., Gomberg, J., ... & Wirth, E. (2021). Toward an integrative geological and geophysical view of Cascadia subduction zone earthquakes. *Annual Review of Earth and Planetary Sciences*, 49, 367-398.

This Article is brought to you for free and open access. It has been accepted for inclusion in Geology Faculty Publications and Presentations by an authorized administrator of PDXScholar. Please contact us if we can make this document more accessible: pdxscholar@pdx.edu.

Authors

Maureen A.L. Walton, Lydia M. Staisch, Tina Dura, Jessie K. Pearl, Brian Sherrod, Joan Gomberg, Simon Engelhart, Ray E. Wells, and multiple additional authors

Annual Review of Earth and Planetary Sciences
**Toward an Integrative Geological
 and Geophysical View of
 Cascadia Subduction Zone
 Earthquakes**

Maureen A.L. Walton,^{1,*} Lydia M. Staisch,^{2,3,*}
 Tina Dura,⁴ Jessie K. Pearl,³ Brian Sherrod,³
 Joan Gomberg,³ Simon Engelhart,⁵ Anne Tréhu,⁶
 Janet Watt,¹ Jon Perkins,⁷ Robert C. Witter,⁸
 Noel Bartlow,⁹ Chris Goldfinger,⁶ Harvey Kelsey,¹⁰
 Ann E. Morey,⁶ Valerie J. Sahakian,¹¹ Harold Tobin,¹²
 Kelin Wang,¹³ Ray Wells,² and Erin Wirth³

¹Pacific Coastal and Marine Science Center, US Geological Survey, Santa Cruz, California 95060, USA; email: mwalton@usgs.gov

²Geology Minerals Energy and Geophysics Science Center, US Geological Survey, Portland, Oregon 97201, USA; email: lstaisch@usgs.gov

³Earthquake Science Center, US Geological Survey, Seattle, Washington 98104, USA

⁴Department of Geosciences, Virginia Tech, Blacksburg, Virginia 24061, USA

⁵Department of Geography, University of Durham, Durham DH1 3LE, United Kingdom

⁶College of Earth, Ocean, and Atmospheric Sciences, Oregon State University, Corvallis, Oregon 97331, USA

⁷Geology Minerals Energy and Geophysics Science Center, US Geological Survey, Moffett Field, California 94035, USA

⁸Alaska Science Center, US Geological Survey, Anchorage, Alaska 99508, USA

⁹Department of Geology, University of Kansas, Lawrence, Kansas 66045, USA

¹⁰Department of Geology, Humboldt State University, Arcata, California 95521, USA

¹¹Department of Earth Sciences, University of Oregon, Eugene, Oregon 97403, USA

¹²Department of Earth and Space Sciences, University of Washington, Seattle, Washington 98195, USA

¹³Pacific Geoscience Centre, Geological Survey of Canada, Sidney, British Columbia V8L 4B2, Canada

**ANNUAL
REVIEWS CONNECT**

www.annualreviews.org

- Download figures
- Navigate cited references
- Keyword search
- Explore related articles
- Share via email or social media

Annu. Rev. Earth Planet. Sci. 2021. 49:367–98

First published as a Review in Advance on
 January 5, 2021

The *Annual Review of Earth and Planetary Sciences* is
 online at earth.annualreviews.org

<https://doi.org/10.1146/annurev-earth-071620-065605>

Copyright © 2021 by Annual Reviews.
 All rights reserved

*These authors contributed equally to this article

Keywords

subduction zone, Pacific Northwest, earthquake, recurrence, megathrust

Abstract

The Cascadia subduction zone (CSZ) is an exceptional geologic environment for recording evidence of land-level changes, tsunamis, and ground motion that reveals at least 19 great megathrust earthquakes over the past 10 kyr. Such earthquakes are among the most impactful natural hazards on Earth, transcend national boundaries, and can have global impact.

Reducing the societal impacts of future events in the US Pacific Northwest and coastal British Columbia, Canada, requires improved scientific understanding of megathrust earthquake rupture, recurrence, and corresponding hazards. Despite substantial knowledge gained from decades of research, large uncertainties remain about the characteristics and frequencies of past CSZ earthquakes. In this review, we summarize geological, geophysical, and instrumental evidence relevant to understanding megathrust earthquakes along the CSZ and associated uncertainties. We discuss how the evidence constrains various models of great megathrust earthquake recurrence in Cascadia and identify potential paths forward for the earthquake science community.

- Despite outstanding geologic records of past megathrust events, large uncertainty of the magnitude and frequency of CSZ earthquakes remains.
- This review outlines current knowledge and promising future directions to address outstanding questions on CSZ rupture characteristics and recurrence.
- Integration of diverse data sets with attention to the geologic processes that create different records has potential to lead to major progress.

1. INTRODUCTION

Subduction zones, where tectonic plates converge along plate boundary megathrust faults, produce some of the most devastating natural disasters globally: great ($M > 8.0$) megathrust earthquakes and their corresponding hazardous phenomena (**Figure 1**). The 2004 $M9.2$ Sumatra earthquake and tsunami killed 250,000 people in 15 countries, producing an international disaster. Even well-prepared countries can suffer catastrophic damage and loss of life, as in the 2011 $Mw9.0$ Tōhoku-Oki earthquake and tsunami in Japan (McGuire et al. 2017). These two catastrophes took the world by surprise and showed a need for better understanding of the seismic cycle and rupture variability in subduction zones. The Cascadia subduction zone (CSZ) of western North America (**Figure 1**) presents a unique opportunity to address major outstanding questions in subduction zone science (Gomberg et al. 2017). With better understanding of these powerful and complicated tectonic systems, we may improve future hazard preparation and maintain the safety and economic viability of affected populations.

Classic elastic theory (Reid 1910) describes the subduction zone seismic cycle as a two-stage model in which the crust and uppermost mantle deform elastically in response to far-field tectonic forces: (a) an interseismic period when strain accumulates (**Figure 2a**) and (b) a coseismic period when an earthquake suddenly relieves the accumulated strain (**Figure 2b**). For a shallow-dipping subduction megathrust, gradual subsidence near the fault and uplift farther away characterizes interseismic upper plate deformation (**Figure 2a**) and is followed by abrupt coseismic reversal of the deformation pattern (**Figure 2b**). Global observations, however, reveal that the process of strain accumulation and release on faults is complex and that the recurrence interval for earthquakes can vary along a fault and through space and time (Sieh et al. 2008, Goldfinger et al. 2012, Kulkarni et al. 2013, Nocquet et al. 2017, Bilek & Lay 2018). This presents challenges when trying to calculate future earthquake probabilities in order to prepare for and mitigate impacts from inevitable future events.

The CSZ extends for more than 1,300 km from Cape Mendocino in northern California to Vancouver Island in southwestern British Columbia (McCrorry et al. 2012) and has been accumulating strain for 320 years since the last great earthquake in 1700 CE (Atwater et al. 2005, McCaffrey et al. 2013). The next CSZ earthquake could be another $\sim M9$ that ruptures the entire

Recurrence interval: the average time span between significant earthquake occurrences on a fault or in an earthquake source zone

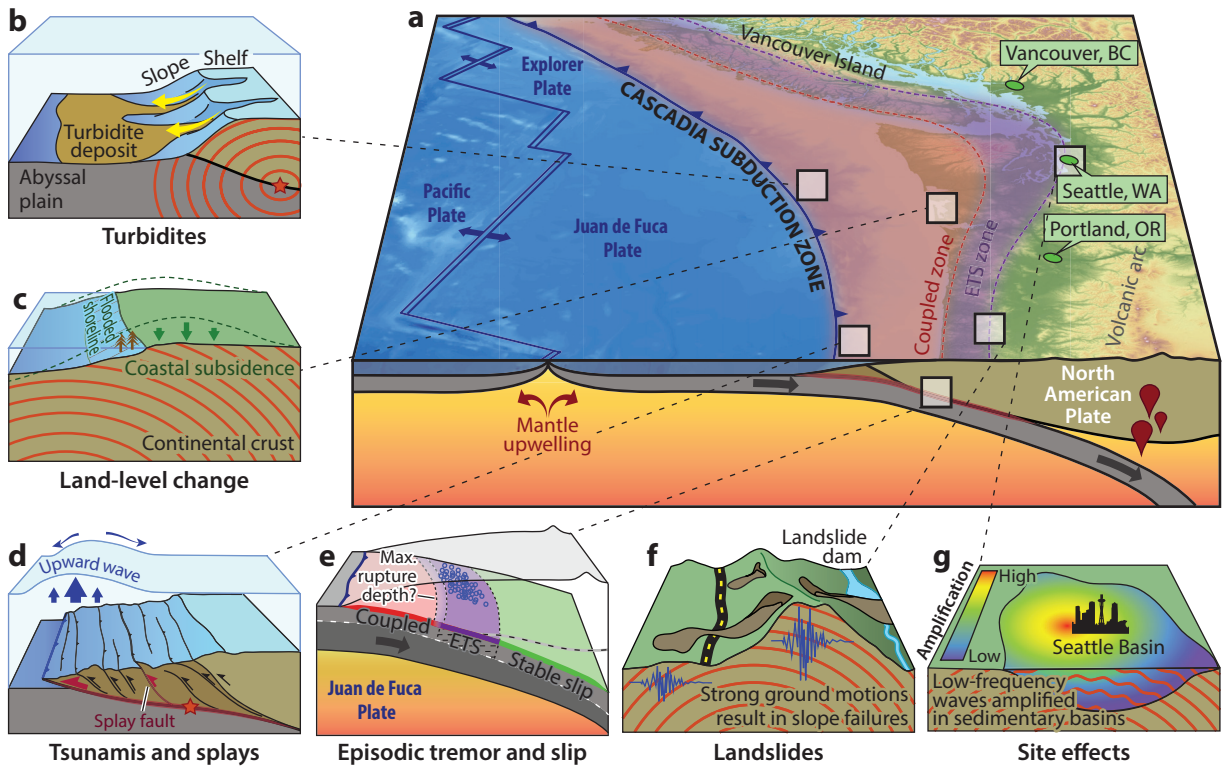


Figure 1

(a) Oblique view of the northwest margin of North America, where the Juan de Fuca and Explorer oceanic plates subduct beneath the North American Plate. On the side view, the thin red line between the two tectonic plates represents the region where great earthquakes occur. On the map overlay, the toothed blue line represents the surface trace of where the subducting plate begins its descent. The purple swath shows the general region where episodic tremor and slip (ETS) occurs, and the pink swath shows the general region considered to be the coupled zone. Small diagrams illustrate various earthquake-related processes labeled beneath each diagram: (b) coseismic turbidite generation; (c) coseismic subsidence with dotted green line showing the pre-event coastal land level; dead brown trees represent marine incursion onto a formerly terrestrial environment; (d) tsunami generation; (e) the relationship between the coupled fault and the ETS zone, with an ETS swarm depicted as blue circles and a possible gap between the coupled zone and up-dip extent of ETS shown as a gradational area; (f) coseismic landslide hazards, with schematic seismograms (in blue) showing the potential for topographic effects on ground motion amplification; and (g) how geologic features, such as sedimentary basins, can amplify seismic waves.

margin like the 1700 CE event but also might be a series of smaller events occurring in quick succession (**Figure 2c**). While recent earthquakes help to inform forecasts of potential earthquakes in other subduction zones (e.g., Alaska in 1946, 1957, 1964, and 1965; Chile in 1960 and 2010; Sumatra in 2004 and 2007; Japan in 2011), geologic records underpin our understanding of earthquake rupture parameters and CSZ earthquake hazard assessments (Hemphill-Haley 1995, Kelsey et al. 2002, Witter et al. 2003, Atwater et al. 2005, Nelson et al. 2008, Goldfinger et al. 2012, Frankel et al. 2015). Fortunately, Cascadia coastal and submarine environments preserve different aspects of past earthquake processes over millennial timescales and feature some of the best prehistoric earthquake catalogs in the world (Hutchinson 1992, Long & Shennan 1998, Goldfinger et al. 2012, Engelhart et al. 2015, Dura et al. 2016a).

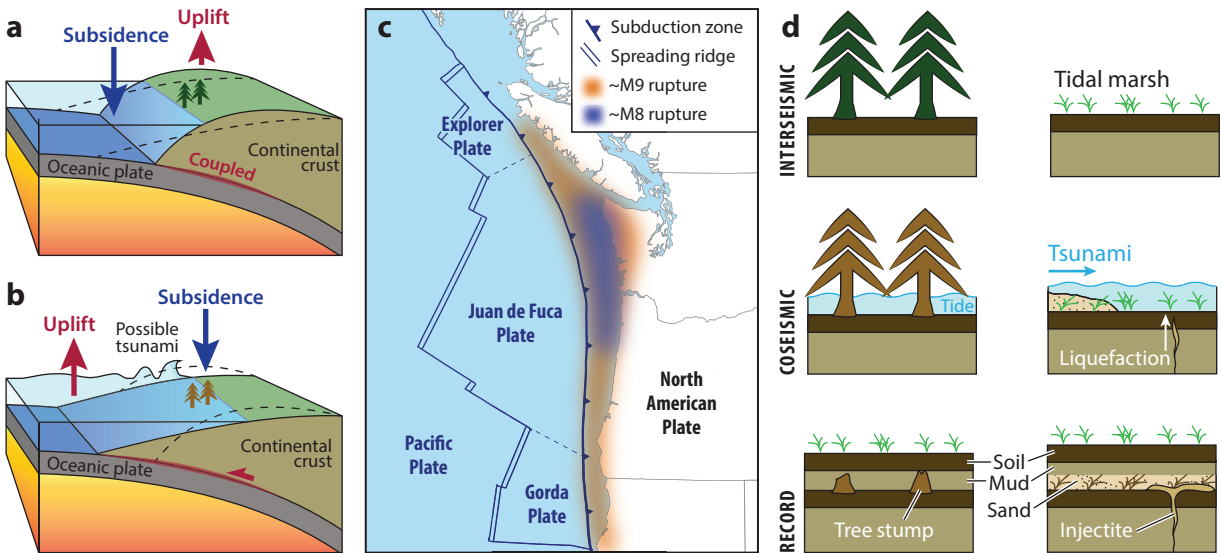


Figure 2

(a) Block diagram of the interseismic period, when convergence along the coupled subduction zone interface (red zone) typically causes gradual uplift in the onshore overriding plate, and gradual subsidence offshore. (b) Diagram of the coseismic period, when earthquake rupture along the subduction zone interface relieves accumulated strain and generally causes sudden subsidence in the onshore overriding plate and sudden uplift in the offshore overriding plate. Shallow rupture may generate a tsunami. (c) Possible scenarios for ~M9 (orange) and ~M8 (blue) events that rupture the Cascadia subduction zone plate interface. (d) Schematic diagrams of stratigraphic evidence for the earthquake deformation cycle, adapted from Atwater et al. (2005). The left column shows the effect of coseismic subsidence on wetland stratigraphy and coastal forests and their preservation in the stratigraphic record (see also **Figure 1c**). The right column shows stratigraphic preservation of coseismic tsunami deposits and liquefaction injectites.

The spatial and temporal robustness of geologic records in Cascadia provides a strong foundation to address outstanding questions on subduction zone science and earthquake recurrence-governing principles that remain elusive globally. However, questions about the timing and extent of past ruptures remain in Cascadia due to age-dating uncertainties resulting in nonunique interpretations of geologic records, unknown relative contributions of coseismic and postseismic motions, and unresolved structural and rheological controls on rupture extent. Furthermore, different rupture characteristics impact tsunami inundation, the extent of seismically triggered landslides, and the effects of geologic architecture on seismic wave amplification (Geist 2002, 2005; Frankel 2013; Frankel et al. 2018; Wirth et al. 2018; Roten et al. 2019; Wirth & Frankel 2019) (**Figure 1**). In this review, we summarize the substantial knowledge gained over decades of subduction zone research in Cascadia, discuss subduction zone processes that create geologic archives of past earthquakes, and identify associated uncertainties and natural variability. We highlight remaining knowledge gaps in CSZ earthquake studies through a synthesis of available data and models and suggest pathways toward accurate interpretation of the earthquake deformation cycle model that incorporates both geological and geophysical data sets.

2. CASCADIA SUBDUCTION ZONE EARTHQUAKE EVIDENCE OVER THE MILLENNIA: GEOLOGIC OBSERVATIONS

The CSZ preserves the most spatially and temporally complete geologic records of past great megathrust earthquakes in the world (Atwater & Hemphill-Haley 1997; Kelsey et al. 2002, 2005;

Witter et al. 2003; Nelson et al. 2006; Goldfinger et al. 2012, 2017). Widespread low-energy, ecologically sensitive tidal wetlands and estuaries and isolated coastal lakes are excellent recorders of decimeter-scale interseismic and coseismic deformation and tsunami inundation (Witter et al. 2003, Engelhart et al. 2015, Dura et al. 2016a) (**Figures 1** and **2d**). Additionally, nearshore marine environments receive ample sediment supply for the generation and preservation of seismically triggered turbidites (Goldfinger et al. 2012) (**Figure 1**). In this section, we summarize existing geologic evidence that constrains the timing and rupture characteristics of past Cascadia megathrust events.

Evidence threshold: criteria that must be exceeded in order to create and preserve a geologic signature of an event (earthquake)

2.1. Onshore Stratigraphic Evidence of the Earthquake Deformation Cycle

The stratigraphy beneath Cascadia's tidal wetlands reflects the strain accumulation and release of the earthquake deformation cycle (**Figure 2d**). Bank sections and sediment cores preserve repeated sequences of organic-rich tidal wetland soils formed in the interseismic period, sharply overlain by tidal mud deposited following decimeter-scale coseismic subsidence (Darienzo et al. 1994, Atwater & Hemphill-Haley 1997, Clague et al. 2000, Kelsey et al. 2002, Witter et al. 2003, Nelson et al. 2008) (**Figure 3a,b**; **Supplemental Table 1**). At some tidal wetland sites, sand and silt layers signaling high-energy tsunami inundation of the coast are evident at the soil-mud contact (**Figures 2d** and **3b**). In coastal lakes, landward-thinning sand beds signal marine incursions from past tsunamis (Kelsey et al. 2005). Radiocarbon ages from pre- and postearthquake and/or tsunami sediment bracket the timing of coseismic subsidence and/or tsunami inundation. Typical age uncertainty is on the order of a few hundred years; however, dendrochronological analysis of trees killed by rapid coseismic subsidence and marine inundation, particularly for events in the past 2,000 years where sufficient wood has been preserved, has the potential to yield more precise ages (Atwater & Yamaguchi 1991; Jacoby et al. 1995, 1997; Yamaguchi et al. 1997) (**Figure 2d**).

Supplemental Material >

The completeness of onshore geologic archives of coseismic subsidence and/or tsunami inundation depends on the creation and preservation thresholds at a site, termed evidence thresholds (Nelson et al. 2006). In order to exceed the creation threshold at a site, the evidence of coseismic subsidence and/or tsunami inundation must be distinct from similar evidence produced by local nonseismic processes (Nelson et al. 2006). In order to exceed the preservation threshold at a site, the balance among erosional and depositional processes must favor the preservation of coseismic subsidence and/or tsunami inundation evidence. Holocene relative sea level (RSL) history and evidence thresholds at each site along the CSZ control the length and completeness of onshore geologic archives of coseismic subsidence and tsunami inundation (Engelhart et al. 2015, Dura et al. 2016a). The longest geologic archives of coseismic subsidence and tsunami inundation are in central and southern Cascadia, where gradual RSL rise since ~5–7 ka produces the accommodation space in tidal wetlands necessary for preservation (Atwater & Hemphill-Haley 1997, Witter et al. 2003). In northern Cascadia (e.g., Vancouver Island), gradual RSL fall since ~6 ka limits the preservation of coseismic subsidence evidence to the last ~1–2 ka, and typically only the last ~500 years (Dura et al. 2016a) (**Figure 4**). Evidence of tsunami inundation in northern Cascadia extends to ~3.5 ka (Goff et al. 2020).

In order to distinguish stratigraphic contacts created by megathrust ruptures from other nonseismic processes (e.g., climate-driven sea-level change, changes in estuary hydrography), researchers consider several criteria: (a) the suddenness of the change in environment across the contacts, (b) the lateral extent of sharp stratigraphic contacts, (c) significant environmental change evident in microfossil assemblages across sharp contacts, (d) the continuity of stratigraphic evidence within a site and across multiple sites, and (e) the coincidence of tsunami deposits with sudden stratigraphic change (Darienzo et al. 1994; Nelson et al. 1996; Shennan et al. 1996, 2016).

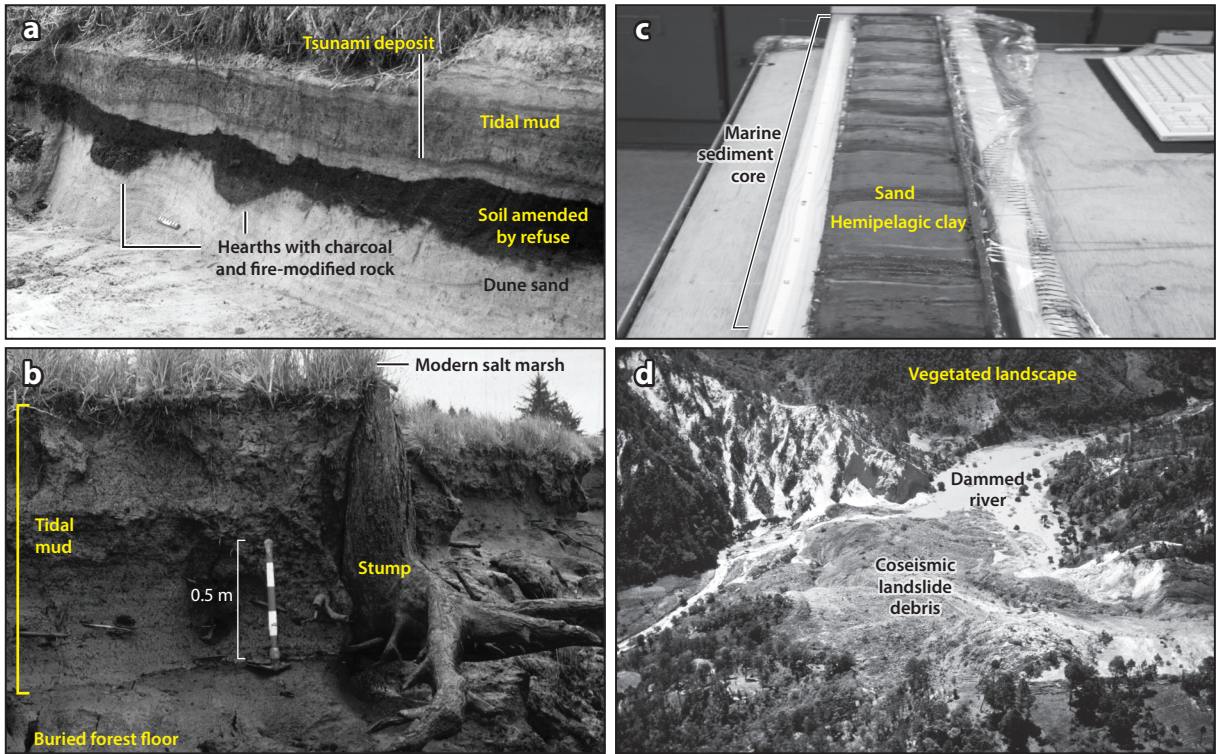


Figure 3

(a) Evidence for coseismic subsidence and tsunami inundation from a sedimentary exposure of subaerial dune sand and prehistoric settlements overlain by tsunami sand and tidal mud along the Salmon River, Oregon. Photo reproduced from Atwater et al. (2005) with permission. (b) Coseismic subsidence evidence from a drowned tree stump surrounded by tidal mud in the Naselle River near Willapa Bay, Washington. Photo reproduced from Atwater et al. (2005) with permission. (c) Marine sediment core showing dark bands of sandy sediment, interpreted as coseismic turbidite deposits, interbedded with lighter-colored hemipelagic clay. Photograph provided by C. Goldfinger. (d) An example of a coseismic landslide that dammed a river to produce a quake lake, from the 1976 Guatemala earthquake. While not an example of coseismic landsliding in Cascadia, this photo demonstrates secondary hazard potential to the Pacific Northwest. Photo reproduced from Espinosa (1976) with permission.

Satisfying the first four criteria implies that an earthquake produced the decimeters of subsidence necessary to exceed the evidence threshold (Nelson et al. 2006). The additional presence of an overlying tsunami deposit (fifth criteria) strongly supports an offshore rupture, rather than localized wetland depositional processes.

The best-preserved and most widely documented megathrust earthquake in the onshore geologic record at the CSZ occurred in 1700 CE (Nelson et al. 1995, Satake et al. 2003, Atwater et al. 2005, Goldfinger et al. 2012) (**Supplemental Text**). Coastal wetlands spanning more than 1,000 km of the CSZ preserve distinct soil-mud contacts and anomalous accompanying silt or sand beds at the contacts that signal sudden coseismic submergence and tsunami inundation of coastal environments (Atwater et al. 2005 and references therein) (**Figures 1 and 2d**). The 1700 CE tsunami propagated across the Pacific, causing inundation and damage along the coast of Japan (Satake et al. 2003, Atwater et al. 2005). Modeling of the arrival time of tsunami waves documented in Japan and dendrochronological dating of coastal trees simultaneously killed by coseismic subsidence in Washington, Oregon, and California precisely constrain the age of the earthquake to

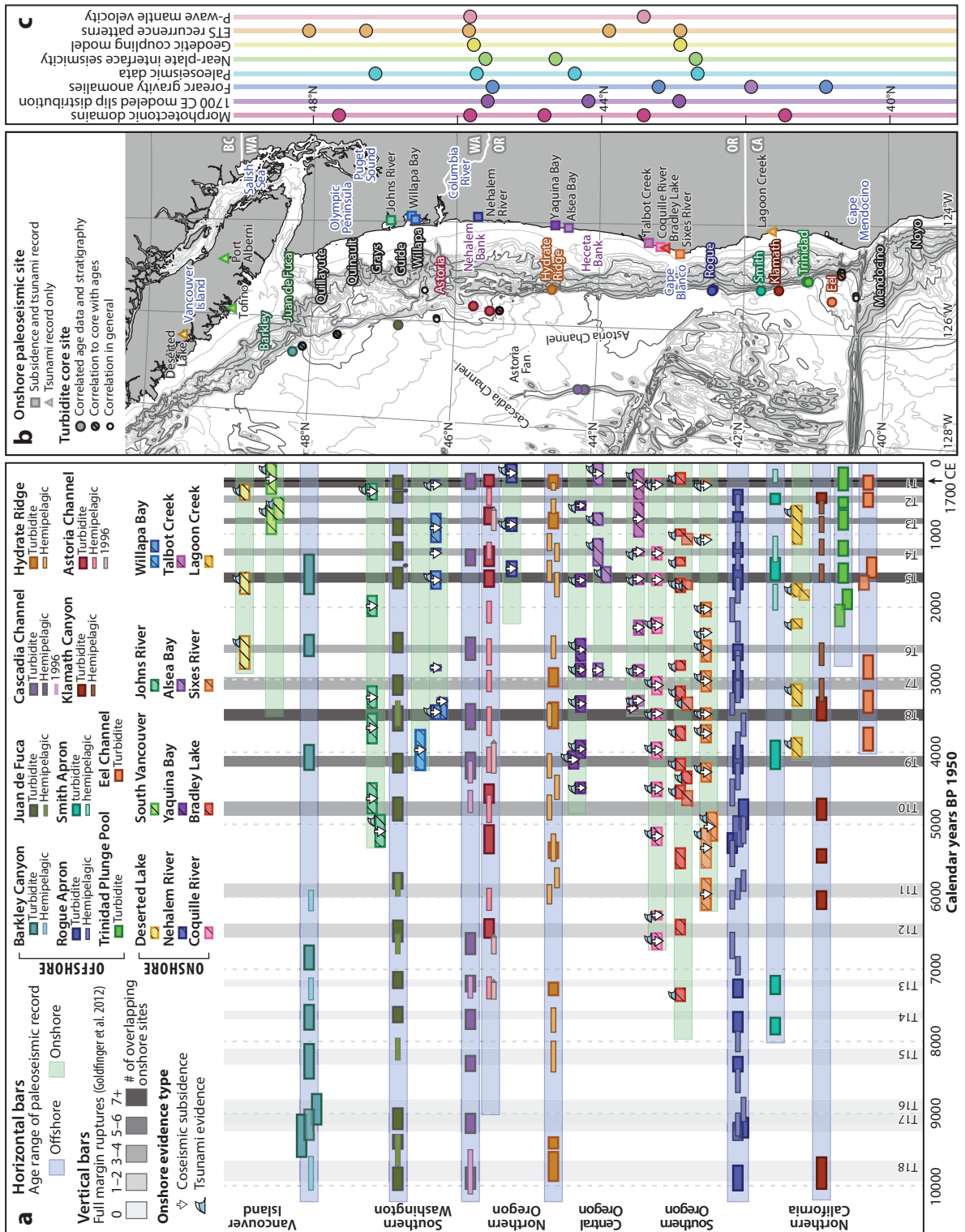
Supplemental Material >

January 26, 1700 CE (Atwater et al. 2005 and references therein). Tsunami modeling, along with the uniquely precise date and concurrence of evidence for this event, supports the inference that it was a full-margin, M8.7–9.2 rupture (Yamaguchi et al. 1997, Satake et al. 2003, Atwater et al. 2005, Nelson et al. 2020).

Stratigraphic- and microfossil-based estimates of coseismic subsidence in 1700 CE aid in assessing the rupture characteristics of the event, such as slip distribution. Early stratigraphic- and microfossil-based estimates of coseismic subsidence in 1700 CE often have uncertainties in excess of a meter (Hemphill-Haley 1995, Dura et al. 2016b), and therefore, highly simplified uniform-slip rupture models were permissible by earlier data sets (Wang et al. 2003; Leonard et al. 2004, 2010). More recent statistically based transfer function analyses use empirical relationships derived from modern foraminifera samples to estimate past marsh elevations from fossil foraminifera assemblages and have reduced subsidence uncertainty to 0.3–0.5 m at some sites (Hawkes et al. 2011, Kemp et al. 2018), although uncertainties due to contamination from possible short-term post-seismic deformation remain (Horton et al. 2017). The more precise microfossil-based subsidence estimates resolve slip variability along the CSZ in 1700 CE and result in more realistic heterogeneous rupture models (Wang et al. 2013, Wirth & Frankel 2019).

Gaining a deeper understanding of recurrence and slip behavior of past events along the CSZ requires geologic records that span multiple earthquake cycles (Leonard et al. 2004, 2010; Wirth & Frankel 2019). Geologic studies in southern Washington and northernmost Oregon tidal wetlands (Shennan et al. 1996, Atwater & Hemphill-Haley 1997, Nelson et al. 2006) document up to 10 widely correlative buried soils representing coseismic subsidence over the past ~5,000 years, with recurrence intervals between earthquakes ranging from a few decades to one millennium (average recurrence 500–540 years). In central and southern Oregon and northern California (Kelsey et al. 2002, Witter et al. 2003, Milker et al. 2016, Padgett et al. 2021), tidal wetlands and coastal lakes preserve up to 12 earthquakes and/or tsunamis over the same ~5,000-year time period (average recurrence ~390 years) (Kelsey et al. 2002, 2005; Witter et al. 2003, 2012b). Geologic records reveal rupture patterns that suggest northern Cascadia commonly breaks in long ruptures, while southernmost Cascadia experiences more frequent ruptures of variable length (Nelson et al. 2006). Geologic records also show variable amounts of subsidence during successive earthquakes at some sites (Milker et al. 2016) and persistent low (Nelson et al. 2021) or high (Kelsey et al. 2002) amounts of deformation at other sites. Along-strike structural barriers at the CSZ (see Section 3.2) potentially control the along-strike variability in rupture length and coseismic deformation over multiple earthquake cycles documented in onshore geologic data sets.

Tsunami deposits can provide clues about the time, location, and extent of the megathrust rupture source that complements other onshore paleoseismic evidence (Peters et al. 2007, Peterson et al. 2011). Earthquake-induced tsunamis occur when coseismic slip causes significant seafloor deformation and are sensitive to the depth and extent of rupture (Priest et al. 2014, Melgar et al. 2016) (**Figure 1d**). CSZ tsunami deposits generally consist of anomalous sandy to silty sediments extending kilometers inland from the shoreline, may contain marine microfossils, and often accompany coastal subsidence records (Kelsey et al. 2002, 2005; Witter et al. 2003) (**Figure 4**). Other tsunamigenic sources, such as crustal earthquakes and large submarine landslides, tend to produce localized tsunamis, whereas megathrust-generated tsunamis affect a broad region (Goldfinger et al. 2000, Garrison-Laney & Miller 2017). At the CSZ, researchers use the inland extent, thickness, and grain size of tsunami deposits preserved along the CSZ to ground truth tsunami inundation simulations (Witter et al. 2013), estimate offshore slip during past tsunamigenic earthquakes (Witter et al. 2012b), and resolve the hydrodynamics of tsunami inundation (Witter et al. 2012a).



(Caption appears on following page)

Figure 4 (Figure appears on preceding page)

(a) Onshore and offshore geologic evidence for CSZ megathrust rupture. Semi-transparent green and blue horizontal bars indicate the temporal length of each record. Onshore and offshore event age range estimates are color-coded with site locations in panel *b*. Offshore age ranges are from turbidites analyzed by Goldfinger et al. (2012). Thick horizontal age ranges are sandy marine turbidite ages estimated from ^{14}C dating of hemipelagic sediments, estimated basal erosion, and inferred sedimentation rate for each geographic locale. Thin horizontal age ranges are calculated ages of interbedded hemipelagic sediment. All age ranges are 2σ uncertainty propagated through ^{14}C age calibration and correction. Vertical gray bars are interpreted event ages from a land-marine age compilation, which takes several onshore geology sites into account with some, but not all, of the geochronologic and stratigraphic information from marine sediment cores (Goldfinger et al. 2012). The shade of gray reflects the number of onshore sites plotted here that are consistent with this interpretation (the darker the color, the more overlapping onshore data). Age ranges for onshore geologic evidence shown with hatched fill. Age ranges for subsidence (*white arrow*) and/or tsunami deposit (*small wave*) events are calibrated ^{14}C dates or from OxCal modeling (**Supplemental Table 2**). (b) Map showing the locations of onshore and offshore study sites; colored location markers correlate with the age ranges in panel *a*. Offshore canyons labeled using white text with colored outlines correlate with turbidite age range bars determined for turbidites associated with that canyon. Black text outlines denote canyon data lacking or not used. Core ID numbers are available in **Supplemental Figure 1**. Marine cores shown are only those used for age dating or stratigraphic correlation (additional marine core locations are available in Goldfinger et al. 2012). Nearshore geographic features are labeled in purple. Onshore geographic features are labeled in blue. Bathymetric contours are 100-m spacing in light gray and 500-m intervals in dark gray (derived from Wong & Grim 2015). (c) North-south evidence for possible rupture boundaries inferred from geophysical data sets, adapted from Watt & Brothers (2021). Circles denote locations of observations of along-strike heterogeneities. Latitudes correspond to the map in panel *b*. Abbreviations: CSZ, Cascadia subduction zone; ETS, episodic tremor and slip.

2.2. Marine Turbidite Records

Marine sediment cores in Cascadia record disturbance layers and evidence for turbidity currents, termed turbidites, generated from offshore coseismic ground shaking (Adams 1990, Goldfinger et al. 2012) (**Figure 1b**). Turbidites can be found in abyssal channels, proximal canyons, fan systems, aprons, and slope basins, and they typically consist of a sharp basal contact; a fine sandy-silty basal layer; and an upward-fining sequence of silt, mud, and clay (**Figure 3c**). In southern Cascadia, subduced mud turbidites lack a sandy component in some locales (Goldfinger et al. 2012, 2013b).

Turbidites result from the shaking produced by megathrust and crustal earthquakes, as well as nonearthquake-related processes such as storms (Goldfinger et al. 2012, Gavey et al. 2017, Howarth et al. 2018, Mountjoy et al. 2018); thus, distinguishing between multiple sources of event beds requires sedimentological arguments or physical criteria, often site specific. One physiographic test is to look for consistent Holocene stratigraphy among site types that lack connections to each other or to terrestrial sources. The confluence test is another physiographic criterion used along the Cascadia margin where multiple channel systems and turbidity current pathways lead away from the filled trench. The confluence argument suggests that if the turbidity currents travel synchronously down the tributary channels and coalesce into a single channel to travel as one large turbidity current, then a margin-wide event, such as a great earthquake, likely triggered the density flows (Adams 1990, Goldfinger et al. 2012). If multiple events trigger turbidity currents, then the tributary channels and the main channel should contain different numbers of turbidite deposits.

Most of the canyon systems of Cascadia are Pleistocene features, making Cascadia an ideal site for Holocene paleoseismology, although there remains some debate about the Pleistocene to modern sediment routing in offshore channels and the infallibility of the confluence test (Atwater & Griggs 2012, Atwater et al. 2014, Hill et al. 2020). While Holocene sediment supply is variable along the CSZ margin and can take a series of complex pathways that could obfuscate estimates of recurrence from the turbidite record (Atwater et al. 2014), Goldfinger et al. (2017) argue that consistent event-bed records among many site types and locales show that the earthquake signal commonly overprints local variability (see also Rong et al. 2014).

Supplemental Material >

Turbidites: disturbance layers and evidence for turbidity currents (density flows) in marine or lacustrine environments

Mud turbidites: turbidite deposits that lack a sandy component

Confluence test: a physiographic criterion used to correlate turbidites across a margin by comparing deposits in tributary and master channels

Multiple tributaries to the Cascadia Channel contain 19 Holocene sandy turbidites, 13 of which postdate the ~7,630-year-old Mazama Ash (Adams 1990, Goldfinger et al. 2012) (**Figure 4**). Downstream, the count remains 13 post-Mazama events in most cores, suggesting synchronous deposition. Heavy mineral suites and hydrodynamic modeling support the independence of the tributaries (Goldfinger et al. 2017) and the Adams (1990) confluence test. Juan de Fuca Channel, Hydrate Ridge slope basin, Rogue Apron, and Astoria Fan each contain 19 sandy turbidites (**Figure 4**). These sandy turbidites share a common chronology estimated from ^{14}C ages and depositional age models, and log correlation methods assist in correlating them along strike (Goldfinger et al. 2012, 2017; Enkin et al. 2013; Hamilton et al. 2015). The 1700 CE earthquake is the youngest turbidite in nearly all marine cores (**Figure 4**). Compilation of turbidite events and onshore subsidence and tsunami records suggests a recurrence interval of 500–530 years for margin-wide (~M9) megathrust earthquakes (Goldfinger et al. 2012). In southern Cascadia at Hydrate Ridge, Rogue Apron, and sites extending to Eel Canyon, a series of 12–22 fine-grained turbidites intercalated between hemipelagic sediments and sandy turbidites have been interpreted as more frequent and limited southern CSZ rupture (Goldfinger et al. 2012).

Turbidite age estimates broadly overlap age ranges for onshore CSZ earthquake evidence, especially for the sandy turbidites representing the largest, most widespread events (Witter et al. 2012b); however, some turbidites interpreted as earthquake-triggered events (e.g., T2) do not have corresponding onshore subsidence or tsunami evidence (**Figure 4**). Differences in evidence thresholds can account for at least some discrepancies between onshore and offshore records (Nelson et al. 2006, Goldfinger et al. 2016). Onshore, subsidence thresholds may be as large as Mw8.4 (Nelson et al. 2006), while the turbidite record includes events at least as low as Mw7.1 (Goldfinger & Gutierrez 2019). For example, mud turbidites above the 1700 CE turbidite layer near Cape Mendocino likely correlate with the 1906 San Andreas and 1992 Petrolia earthquakes, suggesting that crustal $M > 7$ earthquakes triggered these turbidity flows (Goldfinger & Gutierrez 2019). Thus, the turbidite record in southernmost Cascadia appears to include shorter CSZ ruptures as well as crustal earthquakes. The discrepancies in the data sets may alternatively suggest that not all margin-wide turbidites are seismically triggered, or that certain rupture characteristics optimize turbidite generation but do not generate onshore deformation and tsunamis.

2.3. Lacustrine Turbidites and Disturbance Deposits

Lakes from a variety of settings are uniquely sensitive to shaking from different types of seismic sources and often provide long, continuous sediment records ideally suited for paleoseismic investigation (Praet et al. 2017, Moernaut et al. 2018, van Daele et al. 2019, Vandekerckhove et al. 2020); recent research indicates increasing utilization of lacustrine records in Cascadia earthquake science (Morey et al. 2013, Goldfinger et al. 2017, Leithold et al. 2018). Turbidites in Oregon and northern California lakes are of a similar timing and frequency (Morey et al. 2013) as the record of offshore seismogenic turbidites (Goldfinger et al. 2012).

Several studies suggest that lake sediments record locally generated ground shaking magnitude and source. Sedimentary records from Lake Washington, near Seattle, contain two event layers that coincide with known earthquakes, including the 1700 CE megathrust earthquake and an ~1,100-year-old Seattle fault zone rupture; the other six events found in these records are from older earthquakes in the region and have recurrence intervals between 400 and 500 years, which may therefore indicate they were generated by megathrust rupture (Karlin et al. 2004). On the Olympic Peninsula, Lake Quinalt sedimentary records contain three event layers in the past 3,000 years (Leithold et al. 2018), suggesting either that only some CSZ earthquakes cause local ground shaking sufficient to create lacustrine disturbance events or that not all lakes are equally

good earthquake recorders. Also on the Olympic Peninsula, Lake Crescent contains a sedimentary record with four major disturbance events that correlate to rupture along a nearby crustal fault, whereas thinner lake turbidite layers may be from megathrust, upper plate, and intraplate earthquakes that caused lesser local ground shaking (Leithold et al. 2019). On Vancouver Island, Effingham and Saanich Inlets are deep anoxic inlets that effectively mimic lacustrine environments. Of the two records, the Saanich Inlet, well inland, shows evidence for nearly twice as many events (Blais-Stevens et al. 2011), whereas the Effingham Inlet seems to record mainly plate boundary events. In addition, the Saanich Inlet record may suggest that some CSZ megathrust earthquakes rupture only the northern portion of the megathrust (Blais-Stevens et al. 2011). The difference in these records highlights the sensitivity of local response to seismic source type and shaking characteristics.

2.4. Other Onland Proxies of Strong Ground Shaking

Liquefaction from seismic shaking manifests as sedimentary intrusions (sills and dikes), vented sand deposits (**Figure 2d**), soft sediment deformation, and lateral spreading. Previous surveys identify rare surficial liquefaction features in Cascadia (Obermeier 1995, Takada & Atwater 2004). Most evidence for seismically induced liquefaction in Cascadia comes from sedimentary outcrops along rivers and estuaries, such as swampy islands along the lower Columbia River and cut banks of the Chehalis River in southwestern Washington (Obermeier et al. 1993, Atwater 1994, Obermeier 1995, Obermeier & Dickenson 2000, Takada & Atwater 2004). Atwater (1994) describes outcrops on the banks on these islands with hundreds of centimeter-scale sand bodies intruding and, in some cases, venting onto the surface of a buried soil dated to the 1700 CE megathrust earthquake. Slices of subsurface deposits from the lower Columbia River show evidence of liquefaction from at least four great earthquakes in the past 2,000 years (Takada & Atwater 2004).

Subduction zone earthquakes sometimes radiate strong shaking and trigger landslides over broad areas (**Figures 1f** and **3d**), as seen in the 1960 Chilean, 1964 Alaska, and 2011 Tōhoku-Oki earthquakes (Hansen 1965, Veblen & Ashton 1978, Wartman et al. 2013). Researchers have yet to definitively connect any of Cascadia's abundant landslides to a megathrust rupture despite thorough surveys (Perkins et al. 2018, Hill et al. 2020, LaHusen et al. 2020, Struble et al. 2020). The paucity of megathrust-triggered deep-seated landslides along the Cascadia margin may suggest that onshore ground shaking from past great earthquakes was not sufficiently strong. However, recent research suggests landslides from crustal earthquakes or major rainfall events overprint prior potential megathrust-generated landslides (LaHusen et al. 2020, Struble et al. 2020).

Candidate megathrust-generated landslides include rock slides near Newport, Oregon, where modern observations of landslide reactivation rates suggest that it began moving around 1700 CE and continues to move today (Schulz et al. 2012). On the Olympic Peninsula, a terrace formed from a breached rockslide-dammed lake containing buried trees in growth position (Leithold et al. 2018) and a landslide-buried Makah fishing village (Kirk 2015) may correlate to the 1700 CE event. Confirming seismic triggers for these sites requires robust age control.

3. CONTEMPORARY DEFORMATION: CONSTRAINTS FROM INSTRUMENTAL AND GEOPHYSICAL DATA SETS

Determining whether geological boundaries are present and their impact on rupture propagation and megathrust behavior is a major challenge that requires integrating paleoseismic and contemporary geophysical data and comparing the CSZ to other subduction zones. In this section, we review evidence of interplate coupling and contemporary indications of seismic activity in the forearc and discuss what we can infer about earthquake behavior from seismic and geodetic

Seismogenic zone:

the part of the plate boundary located from ~15 to 35 km depths that tends to rupture in large earthquakes

Stick-slip behavior:

the frictional behavior required to generate an earthquake; where dynamic friction is less than the static friction

Coupled zone:

a geodetically inferred proxy for the seismogenic zone

Rupture patch:

the area on the megathrust that slips during a particular earthquake

Rupture boundaries:

heterogeneities in physical properties that may inhibit earthquake rupture propagation over multiple earthquake cycles

Tsunami**earthquakes:**

earthquakes in which shallow (depths less than ~15 km) slip occurs offshore, generating tsunamis

observations. We use several terms to describe portions of the subduction zone exhibiting common slip behavior; because some studies use these terms differently, we define them here as follows. The seismogenic zone is the part of the plate boundary where dynamic friction is less than the static friction and exhibits stick-slip behavior. This behavior is a prerequisite for generating an earthquake. The coupled zone is a proxy for the seismogenic zone and is the part of the plate boundary that has geodetically inferred slip deficit and appears to be storing elastic energy. We define a rupture patch as the area on the megathrust that slips during a particular earthquake. We discuss evidence for and against geologically controlled rupture boundaries on the megathrust that may define persistent, recurrent rupture patches.

Accurate CSZ megathrust earthquake scenarios hinge on our understanding of the existence and persistence of rupture boundaries, both along strike and down dip, and the structural or rheologic properties that modulate these boundaries. Heterogeneities evident in proxies for megathrust behavior may sometimes indicate spatially persistent rupture characteristics such as slip or rupture boundaries. We note that potential boundaries do not necessarily inhibit all ruptures, depending on the physics of rupture propagation (Bilek & Lay 2018). Rupture boundaries may be persistent, frequent, or ephemeral (rarely traversed, occasionally traversed, or always changing, respectively) (Philibosian & Meltzner 2020). For example, the Kii Peninsula in Japan is a boundary along the Nankai-Suruga Trough that impeded throughgoing rupture of the 1944 Tonankai and 1946 Nankai earthquakes, but the 1707 Hōei earthquake ruptured the entire margin (Garrett et al. 2016). While the 1700 CE event in Cascadia was likely an ~M9 earthquake that ruptured the entire length of the CSZ (Atwater et al. 2005), the geologic record likely also preserves smaller earthquakes that rupture only a portion of the subduction zone (Wells et al. 2003, Goldfinger et al. 2012). The long-term persistence of rupture boundaries in Cascadia and elsewhere is an ongoing question (Victor et al. 2011, Meltzner et al. 2012). The geologic record is necessary to verify interpretations of rupture boundaries gleaned from geophysical data, but conversely, along-strike and down-dip patterns evident in instrumental data sets may also help distinguish between conflicting interpretations of rupture boundaries in the geologic record. Below we summarize the three-dimensional variations in the CSZ environment and megathrust slip behaviors that we can observe with modern geophysical instrumentation.

3.1. Depth-Dependent Seismic Behavior and Frictional Properties

All subduction zones exhibit depth-dependent slip behaviors along the plate interface (Lay et al. 2012, Bilek & Lay 2018). In the upper coupled zone, at depths less than ~15 km, strain release generally occurs either largely aseismically or in earthquakes with relatively low amounts of short-period energy radiation and low stress drop (Newman & Okal 1998, Ye et al. 2016, Sahakian et al. 2019), often termed tsunami earthquakes, as they generate tsunamis that are anomalously large for the corresponding earthquake magnitude (Hill et al. 2012, Lay et al. 2012). This zone can rupture coseismically during megathrust earthquakes (e.g., the 2011 Mw9.0 Tōhoku-Oki and 2010 Mw8.8 Maule events). From ~15–35 km depths, earthquakes can produce large slip and emit broadband seismic waves, although the size of individual rupture patches and amount of slip in each event vary in space and time (Lay et al. 2012, Bilek & Lay 2018). A transitional zone below ~35 km depth exhibits various types of slow-slip behaviors, including slow-slip events (SSEs) in which several centimeters of slip occur over a large area over a period of days to years (Obara & Kato 2016, Bilek & Lay 2018, Bartlow 2020). These events occur near where the downgoing plate meets the hydrated mantle wedge (Obara & Kato 2016, Gao & Wang 2017). Debates persist over the exact relationships between and physical controls on these depth zones in Cascadia and elsewhere (Obara & Kato 2016, Wang & Tréhu 2016, Gao & Wang 2017).

Limited seafloor geodetic observations and an exceptionally low rate of low-magnitude background interplate seismicity in the CSZ blur our understanding of the geometry and depth of the seismogenic zone and the degree of interseismic coupling (Wang & Tréhu 2016). The relative lack of seismicity, along with inversion of geodetic data sets, suggests that the CSZ seismogenic zone is nearly fully coupled along much of its length, although the width and degree of coupling may vary along strike; notably, central Cascadia has been modeled as both an anomalously narrow zone of coupling and a wide zone of partial coupling (McCaffrey et al. 2013, Schmalzle et al. 2014, Pollitz & Evans 2017, Li et al. 2018, Michel et al. 2018) (**Figure 5**). Calculated Holocene vertical land motion most closely matches models that include a fully coupled CSZ at shallow (<30 km) depths (Yousefi et al. 2020) (**Figure 5**). In general, the width of the inferred seismogenic zone in Cascadia decreases to the south, potentially impacting megathrust earthquake slip magnitude, an interpretation that is consistent with the apparent increase in megathrust event frequency from the geologic record (Scholz 2014, Tréhu 2016). The recent and planned installation of offshore global navigation satellite system acoustic (GNSS-A) instrumentation should reduce the nonuniqueness of coupling models by helping to constrain offshore strain accumulation (Bürgmann & Chadwell 2014, Heeseemann et al. 2017, Chadwell et al. 2018) (**Figure 5**). Initial data from these GNSS-A sites indicate a high degree of near-trench coupling (Chadwell et al. 2018).

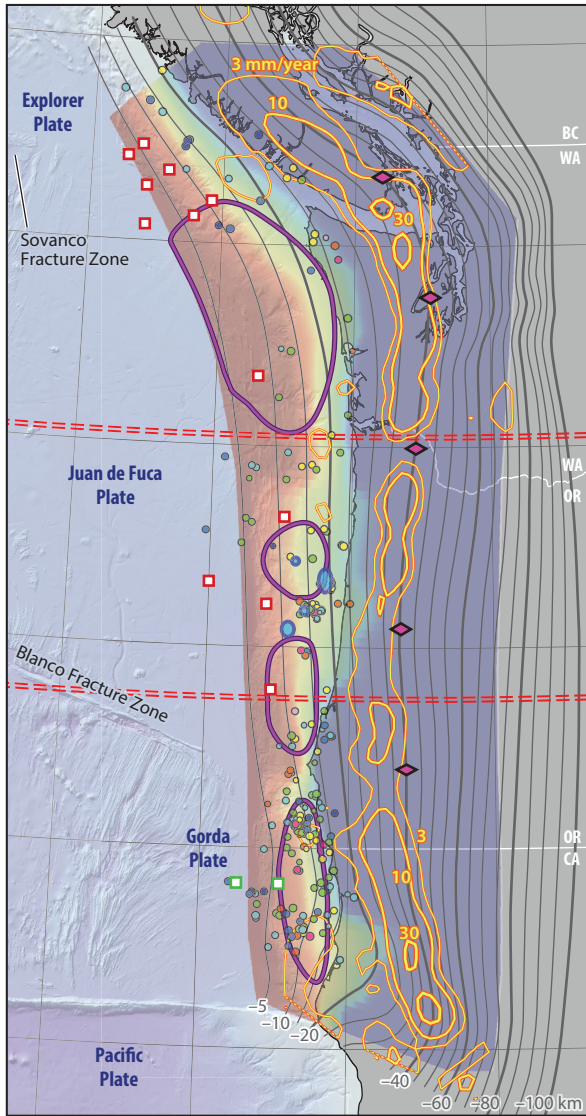
Direct observations of earthquakes in other subduction zones inform our understanding of CSZ rupture processes. Ground motion observations from the 2011 Mw9.0 Tōhoku-Oki and 2010 Mw8.8 Maule events suggest that the frequency content of the radiated seismic energy varies with depth within the seismogenic zone. Ground motions from these two events can be explained by incorporating high-stress-drop subevents, which are M8-size rupture patches at 20–30-km depths superimposed on the lower-stress-drop background slip (Wang & Mori 2011, Frankel 2013). Recent CSZ ~M9 rupture models include such subevents (Frankel et al. 2018, Wirth et al. 2018) and are compatible with variability in 1700 CE coseismic subsidence estimates (Wirth & Frankel 2019). Inclusion of modeled high-stress-drop subevents impacts slip patterns, ground motions, upper plate structure, and interpretation of ground shaking proxies in the geologic record, although their full impact requires further investigation. Shallow (depths less than ~10–15 km) tsunami earthquakes typically exhibit much weaker shaking (Sahakian et al. 2019), but the resulting slip distribution and seafloor deformation from shallow earthquakes are also critical controls on coseismic hazards, specifically tsunami inundation (Priest et al. 2014, Melgar et al. 2016).

Seismically and geodetically measured slow-slip and tremor phenomena, termed episodic tremor and slip (ETS), occur with remarkable regularity along the CSZ (Dragert et al. 2001, Rogers & Dragert 2003, Brudzinski & Allen 2007, Gomberg 2010, Boyarko et al. 2015, Wells et al. 2017, Bartlow 2020) (**Figure 1e**). ETS occurs at ~30–50 km depths, below the seismically coupled zone, with a creeping gap between the base of the coupled zone and the slow-slip zone (Hyndman et al. 2015, Bruhat & Segall 2016, Bartlow 2020) (**Figure 1e**). Slow-slip and tremor phenomena migrate together, suggesting that these phenomena are different manifestations of the same seismic process (Bartlow et al. 2011). Although we currently do not fully understand the exact physical controls on slow slip and its relationship to geodetic coupling, high pore fluid pressures near the mantle wedge may be responsible for generating slow slip here (Hyndman et al. 2015, Wang & Tréhu 2016, Gao & Wang 2017). Globally, SSEs generally occur along megathrust interfaces that have relatively young downgoing oceanic lithosphere (Lay et al. 2012). SSEs do not accommodate the full slip budget along most of the subduction zone, implying significant inter-SSE creep may occur on the interface within the SSE zone (Bartlow 2020). Whether any slip deficit in this depth range will contribute to slip during a future CSZ megathrust earthquake remains a mystery, and the degree to which stresses from SSEs may be important in triggering the

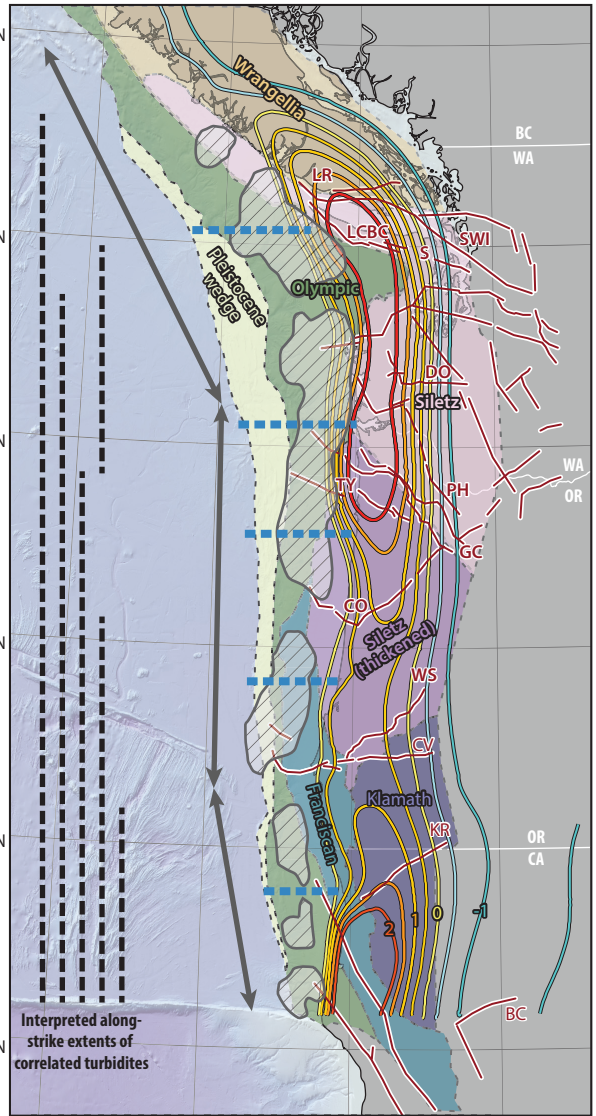
Episodic tremor and slip (ETS):

the phenomenon of seismically measured tremor that accompanies geodetically observed slip along a plate interface

Incoming plate/plate interface



Overriding plate



- AD 1700 8-m+ slip patch (Wang et al. 2013)
- Subducted seamounts (Tréhu et al. 2012)
- ◆ Apparent ETS segments (Brudzinski & Allen 2007)
- ETS slip rate (mm/year) (Bartlow 2020)
- Slab contours (km) (McCrory et al. 2012)
- - - Slab buoyancy (Bodmer et al. 2018)
- Coupling fraction (Schmalzle et al. 2014)
- Offshore GNSS sites (Active □ Planned)
- Seismicity, M (Stone et al. 2018)
- Depth (km)
- Turbidite event extents (Goldfinger et al. 2012)
- Crustal faults (Wells et al. 2017)
- ▨ Interseismic VLM (mm/year) (Yousefi et al. 2020)
- ↔ Change in margin strike
- Terranes (Watt & Brothers 2021)
- Gravity lows (Wells et al. 2003)
- ▨ Morphotectonic boundary (Watt & Brothers 2021)

(Caption appears on following page)

Figure 5 (Figure appears on preceding page)

Maps of geophysical and geologic data sets used to infer along-strike heterogeneities along the CSZ. (a) Heterogeneities on the incoming plate and plate interface. Time-averaged ETS slip rates from Bartlow (2020) are shown as orange contours with values of 30, 10, and 3 mm/year. Slab contours are shown as gray lines with values from -5 to -100 km. Seismicity from Stone et al. (2018) shows events associated with the CSZ, although note that earthquake depths are poorly constrained and some events may be located within the upper plate. Dense clusters of seismicity near latitudes 44.3° and 44.6°N are coincident with subducted seamounts interpreted from magnetic and gravity anomalies (Tréhu et al. 2012). (b) Heterogeneities on the overriding plate. Morphotectonic zones inferred do not necessarily have sharp boundaries (Watt & Brothers 2021). Abbreviations: BC, Battle Creek fault; CO, Corvallis fault; CR, Columbia River fault; CSZ, Cascadia subduction zone; CV, Canyonville fault; DO, Doty fault; ETS, episodic tremor and slip; GC, Gales Creek fault; GNSS, global navigation satellite system; KR, Klamath River lineament; LCBC, Lake Creek Boundary Creek fault; LR, Leech River fault; PH, Portland Hills fault; S, Seattle fault; SWI, South Whidbey Island fault; TY, Tillamook-Yamhill fault; VLM, vertical land motion; WS, Wildlife Safari fault. The bathymetric base layer was adapted from Wong & Grim (2015).

next great earthquake in Cascadia is a matter of current debate (Mazzotti & Adams 2004, Beeler et al. 2014, Bartlow 2020).

3.2. Along-Strike Variability in Slip Behavior and Structure

Many geophysical imaging studies in Cascadia indicate that along-strike heterogeneity exists in forearc upper plate crustal structure. For example, the early Eocene-age Siletz/Crescent terrane that forms the crystalline basement throughout much of the Cascadia forearc (**Figure 5**) is unusually thick and extends offshore between $\sim 43^\circ$ and 46°N . The unique composition of this terrane and other crystalline terranes within Cascadia has been correlated with along-strike variations in upper plate seismicity, ETS periodicity and slip, degree of coupling, and other factors (Tréhu et al. 1994, 2012; Wells et al. 1998, 2003; Brudzinski & Allen 2007; Porritt et al. 2011; Li & Liu 2016; Bartlow 2020) (**Figure 5**). The Siletz terrane exists along the stretch of central Cascadia where geodetic models show a narrow, fully coupled zone or a wide, partially coupled zone (Schmalzle et al. 2014) (**Figure 5**). Wells et al. (2017) speculated that upper plate faults in the brittle Siletz terrane reduce fluid overpressure and deoptimize tremor conditions. In a comprehensive examination of the tectonic geomorphology, outer wedge taper, and seaward and landward structural vergence along the accretionary complex, Watt & Brothers (2021) concluded that along-strike variations in shallow megathrust behavior correlate with upper plate structural boundaries and suggested that the thickened Siletz terrane acts as a backstop influencing the frictional properties of the megathrust through modulation of wedge strength (**Figures 4 and 5**).

In the seismogenic zone, model results for 1700 CE slip distribution constrained by land-level change data (Wang et al. 2013) show possible low-slip regions that correlate with structural boundaries located roughly near $42\text{--}43^\circ$, 44.5° , and 46°N (**Figures 4 and 5**). The degree of coupling along strike may relate to variation in buoyant asthenosphere beneath the downgoing plate; Bodmer et al. (2018) used seismic tomography to argue for decreased buoyancy of the subducting Juan de Fuca Plate between $\sim 43^\circ$ and 46°N , relating it to decreased interplate coupling and non-volcanic tremor at these latitudes (**Figures 4 and 5**). Wells et al. (2003) argued that forearc basins represent basal erosion of the upper plate due to increased frictional strength of the plate boundary, forming potentially recurrent high-slip patches over multiple earthquake cycles (**Figure 5**). Stone et al. (2018) found generally higher rates of forearc seismicity south of 46°N and correlate this with incoming plate roughness and sediment thickness (**Figure 5**). Persistent clusters of seismicity during the past several decades on or near the plate boundary within the seismogenic zone near 44.3° and 44.6°N also correlate with subducted seamounts inferred from potential field and seismic imaging data (Tréhu et al. 2012, 2015; Morton et al. 2018; Stone et al. 2018) (**Figures 4 and 5**). Tréhu et al. (2012) attributed these clusters to interactions between subducted seamounts and the Siletz terrane.

While numerous geophysical and instrumental data sets reveal along-strike variation of the CSZ, the relevance of these observations for understanding the dynamic behavior of past and future CSZ earthquakes is complex and controversial (Philibosian & Meltzner 2020). Along-strike variations in paleoseismic data (Goldfinger et al. 2017) remain the most direct proxies for past earthquake behavior and to verify boundaries hypothesized from geophysical data. Given the lack of coseismic observations, we cannot immediately resolve the causes for along-strike correlations in geophysical data, and we have limited ability to link inferred changes in frictional properties along the megathrust to slip behavior and long-term strain accumulation patterns in Cascadia. Well-resolved preseismic, coseismic, and postseismic observations on other subduction zones provide a framework for interpreting geophysical and instrumental records in Cascadia. Many studies have modeled and interpreted activity in subduction zone earthquakes in the context of geologic structure (Davis et al. 1983, von Huene & Scholl 1991, Saffer & Bekins 2002, Lamb 2006, Cubas et al. 2013, Fujie et al. 2013, McNeill & Henstock 2014, Bassett et al. 2016, Henstock et al. 2016, Saillard et al. 2017, Tréhu et al. 2019, Olsen et al. 2020). Comparative studies can help to reconcile geophysical observations with the geologic record to best understand CSZ recurrence.

4. RECURRENCE MODELS AND IMPLICATIONS FOR SEISMIC HAZARD

A fundamental aim of CSZ paleoseismic studies is to determine a recurrence model that fits our understanding of past CSZ earthquakes. A well-constrained recurrence model is particularly relevant for probabilistic seismic hazard assessment (PSHA) models, which form the basis for the US National Seismic Hazard Maps (NSHM) (Petersen et al. 2019). PSHA models estimate the probability of ground motion exceedance, termed hazard (Cornell 1968), using input earthquake scenarios describing the slip distribution, fault location, fault geometry, and recurrence. Earthquake recurrence models typically considered for subduction zone margins and other major fault systems are categorized as either time independent or time dependent (**Table 1**).

The time-independent model is a common choice for PSHA models, especially when applied to broad regions with multiple fault systems, because it requires minimal information, namely mean recurrence rate. Often described as a Poisson process, time independence assumes that events occur at a certain mean rate but with random event timing. The time-independent recurrence implies that occurrence is memoryless and hazard is constant, and it may suggest that accumulated far-field stress on the fault system does not define earthquake rupture timing (**Figure 6; Table 1**). The aggregate behavior of a region may appear Poissonian, even if composed of faults with individually time-dependent earthquake recurrence (Cornell & Winterstein 1988).

Time-dependent recurrence assumes that earthquakes rupture with a regularity defined by accumulated stress levels on the fault system. In a periodic model, both the interevent time and slip during each event are predictable and earthquake hazard probabilities increase proximal to the mean recurrence time (Shimazaki & Nakata 1980) (**Figure 6; Table 1**). Idealization of the periodic model suggests common slip magnitude (Schwartz & Coppersmith 1984) (**Figure 6**); however, observations suggest a more flexible definition of the periodic model, with quasi-periodic large ruptures in addition to less periodic moderate events with variable rupture characteristics (Zielke 2018). The clustered model is a subcategory of time-dependent models in which strain energy balances over multiple seismic events followed by a period of seismic quiescence (**Figure 6; Table 1**). Slip rate averaged over multiple earthquake cycles is constant, but fault slip for each event can be variable (**Figure 6**). Nested clusters of subduction zone earthquakes are termed supercycles (Sieh et al. 2008, Goldfinger et al. 2013a, Herrendörfer et al. 2015, Philibosian & Meltzner 2020).

Table 1 Characteristics of different earthquake recurrence models

	Time independent		Time dependent	
	Poisson	Quasi-periodic	Quasi-periodic	Clustered
Event rate and periodicity	There is a general rate of occurrence (e.g., two events per millennium), but events are not periodic.	There is a rate of occurrence, and events are periodic.	There is a rate of occurrence, and events are periodic.	There is a rate of occurrence, and cycles are periodic. However, an earthquake cycle includes multiple superimposed cycles.
Energy balance and stress release	Events are independent of accumulated/released stress.	Single-event cycle with characteristic magnitude releases sufficient accumulated stress to renew the statistical process.	Single-event cycle with characteristic magnitude releases sufficient accumulated stress to renew the statistical process.	Stress accumulation and release balances over an earthquake cluster or supercycle.
Interevent time and probability	Random and unpredictable—interevent time does not depend on slip rates or accumulated stress. There is equal probability for a 2-year and a 200-year interevent time.	Consistent and predictable—interevent time depends on strain accumulation rates. Probability of occurrence increases as mean interevent time approaches.	Consistent and predictable—interevent time depends on strain accumulation rates. Probability of occurrence increases as mean interevent time approaches.	Interevent time depends on whether cluster is complete or in progress. Probability of occurrence increases as either the mean intracenter or extracenter event times approach.
Hazard rate	Constant, independent of last event (memoryless).	Normal distribution around the expected event recurrence.	Normal distribution around the expected event recurrence.	Complex distribution around more than one event recurrence.
Coefficient of variation	~1	<1	<1	>1

In this section, we summarize the methodology and underlying assumptions that differentiate between various recurrence models and, as a thought experiment, explore the range of recurrence models compatible with interpretations of the paleoseismic record. We highlight the difficulty in distinguishing full-margin from serial ruptures in the geologic record and discuss the implications for seismic hazard assessment.

4.1. The Coefficient of Variance and Its Application to the Cascadia Subduction Zone

An outstanding controversy remains in which some argue all events in the paleoseismic record are full-margin M9s and others argue that a portion of those events may be a series of smaller M8s that occur in quick succession irresolvable by geochronologic uncertainties (Atwater et al. 2014, Frankel et al. 2015). Additional uncertainty remains about potential rupture barriers and how to handle partial ruptures along the margin, particularly the more frequent ruptures interpreted in southern Cascadia. Below, we explore how these two outstanding uncertainties may affect the coefficient of variation (*CV*), a simple statistical metric that researchers commonly use to evaluate proposed recurrence models. While not always inclusive of nuanced detail in long paleoseismic records, *CV* values inform hazard analyses on possible recurrence scenarios and thus provide a basis from which to construct hazard models. The equation for *CV* is as follows:

$$CV = \frac{\sigma_{\tau}}{\mu_{\tau}},$$

where σ_{τ} and μ_{τ} are the standard deviation and mean of interevent times, τ , respectively (Cramer et al. 2000, Field 2015) (Table 1). In the time-independent model, random processes lead to similar means and standard deviations; thus, the $CV \approx 1$. In the time-dependent periodic model,

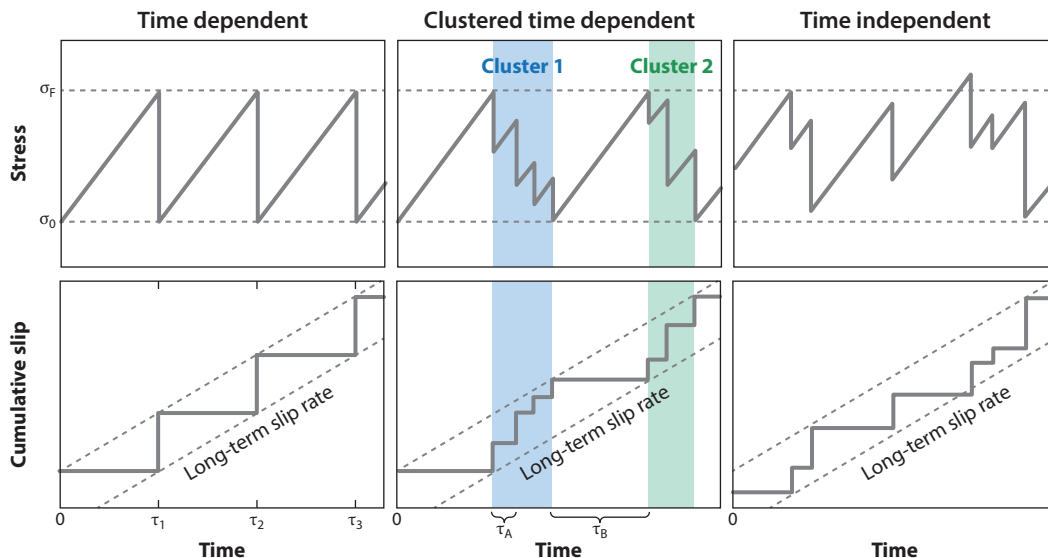


Figure 6

Schematic depiction of recurrence models often proposed for subduction zone settings. (a) The time-dependent model suggests periodic earthquake occurrence is dependent on steady long-term strain accumulation and failure at a critical stress level (i.e., from σ_0 to σ_F). This model suggests predictable slip magnitude. (b) The clustered time-dependent model suggests earthquake recurrence is variable, with clustered occurrence earthquakes punctuated by longer intervals, τ_B , of seismic quiescence. Within a cluster, the probability of recurrence at a return interval of τ_A is high. Following a cluster, probability of recurrence decreases until the onset of the next cluster at a return interval of τ_B . This model suggests that long-term strain accumulation and slip rate may be similar to the periodic model but that slip and timing are less predictable. (c) The time-independent model suggests that earthquake occurrence is unpredictable and may indicate that the displacement rate at the fault trace averaged over several consecutive earthquakes is nonlinear.

consistent interevent times result in a small standard deviation and $CV \leq 1$. $CV \geq 1$ indicates variable interevent times and suggests clustered behavior (Table 1). Application of CV assumes a well-sampled seismic catalog that is long enough to capture typical recurrence behavior. Petersen et al. (2002) evaluated a CV between 0.1 and 0.4 for the Pacific Northwest but included crustal and intraplate events; here we focus on the megathrust to discuss the CSZ earthquake cycle model. Recurrence models and the CV apply to a catalog of significant events, which are fault slip events that release enough stress to permit statistical renewal of the recurrence process. This generally requires a rupture of the full fault system or a large enough rupture to relieve sufficient accumulated stress (Herrendörfer et al. 2015).

Significant events:

fault slip events that relieve enough stress to permit statistical renewal of the recurrence process

4.2. Full-Margin Ruptures

Geoscientists infer 19–20 full-margin \sim M9 CSZ earthquakes over the past 10 kyr from marine and onshore geologic data sets (Goldfinger et al. 2012, 2017; Enkin et al. 2013; Hamilton et al. 2015) (Figure 4). Using this catalog, CV calculations imply time-dependent quasi-periodic recurrence in Cascadia ($CV = 0.51$) (Supplement Tables 3 and 4). If partial-margin ruptures longer than 660 km (Supplement Table 4) are significant and renew the recurrence process, CV reduces to 0.39 (Supplement Table 3). These CV estimates vary insignificantly regardless of whether we include events with weak onshore geologic support (e.g., Table 2; Supplement Table 3). These basic CV calculations strongly suggest a quasi-periodic recurrence model for the CSZ (Supplement Table 3), assuming correlated events are single \sim M9 ruptures. If correct,

Supplemental Material >

the quasi-periodic recurrence model would suggest that the CSZ is currently in the late stages of the earthquake deformation model.

Goldfinger et al. (2012) and Kulkarni et al. (2013) identify temporal gaps after T5, T10, and T15 in the marine record to argue for clustered full-margin event recurrence; however, some onshore events along the margin may fill in these temporal gaps along the margin (e.g., Johns River to Lagoon Creek between T5 and T6; **Figure 4**). The potential for clustered CSZ megathrust earthquakes has important hazard implications (Kulkarni et al. 2013) and therefore merits attention.

4.3. Serial and Partial Ruptures

The uncertainty in ^{14}C dating techniques (tens to hundreds of years) allows for the possibility of interpreting some of the 19–20 correlated events as serial ruptures, in which time intervals smaller than dating uncertainties separate multiple $\sim\text{M8}$ earthquakes (**Figure 2**). Currently, little evidence supports serial rupture as a common seismic occurrence along the CSZ; however, two events captured in the Bradley Lake record that are separated by more than 22 years (Kelsey et al. 2005) correlate to a possible T5 turbidite doublet in Rogue Canyon marine cores (Goldfinger et al. 2012), suggesting serial ruptures may occur occasionally. If we assume one third to one half of the full-margin events interpreted by Goldfinger et al. (2012) are actually three to four serial ruptures separated by 10–100 years (**Supplemental Table 4**), the resulting CV 's suggest Poisson and clustered recurrence models, respectively (**Supplemental Table 3**). We consider only up to half of events as possible serial $\sim\text{M8}$ ruptures, as a majority of $\sim\text{M9}$ ruptures are required to accommodate incoming plate convergence rate seismically (Frankel et al. 2015). These hypothetical rupture scenarios indicate that CV estimates for nonquasi-periodic recurrence are attainable only if a large portion of the geologic record has been misinterpreted as full-margin M9 ruptures.

In addition to uncertainty in full-margin rupture regularity, portions of the CSZ seem to rupture more frequently and may have an earthquake cycle independent of the full-margin cycle. Some geologic data south of Cape Blanco show a striking increase in the number of events recorded and a corresponding decrease in the interevent time (**Figure 4**; **Supplemental Table 3**). The marine core record includes 17 additional events, many from mud turbidites, limited to southern Cascadia (Goldfinger et al. 2012) (**Supplemental Table 3**). Whether these events represent CSZ or crustal earthquakes remains an open question (Goldfinger & Gutierrez 2019). Onshore records indicate 11 events limited to south of Cape Blanco and 2 limited to northern Cascadia (Williams et al. 2005, Nelson et al. 2006, Blais-Stevens et al. 2011) (**Figure 4**). Assuming these smaller ruptures represent CSZ earthquakes, the CV applied to southern Cascadia ruptures implies a time-dependent, quasi-periodic recurrence model (**Supplemental Tables 3 and 4**). The recurrence interval for ruptures limited to northern Cascadia remains elusive (Petersen et al. 2014).

4.4. Implications for the Cascadia Subduction Zone Earthquake Cycle Model

Various rupture scenarios discussed above lead to CV values consistent with interpretation of Poisson, quasi-periodic, and clustered recurrence models for the CSZ. This highlights how current dating uncertainties and debates on rupture variability along the CSZ render an evaluation of the earthquake cycle model in Cascadia premature.

PSHA offers a means of quantifying the intrinsic variability of the system, termed aleatoric variability, and addressing uncertainties that stem from limited knowledge, termed epistemic uncertainty. The current US NSHM uses extensive logic trees that weigh various M8 and M9 rupture

Serial ruptures:

a series of earthquakes on adjacent rupture patches along a margin separated by short time intervals (days to decades)

Aleatoric variability:

the irreducible intrinsic natural variability of a system

Epistemic

uncertainty: reducible uncertainties that stem from limited knowledge

Supplemental Material >

scenarios to define two additive CSZ earthquake scenarios: (a) full margin \sim M9s that recur every \sim 500 years and (b) partial M8.0–8.7 rupture of the CSZ (Frankel et al. 2015). The recurrence rates for partial ruptures in northern and southern Cascadia, which strongly influence hazard, are averaged between different possible scenarios supported by onshore or offshore evidence (Petersen et al. 2014, Frankel et al. 2015). Future updates to the US NSHM may include the possibility of serial rupture (Frankel et al. 2015). Accurate hazard analyses can improve by reducing epistemic uncertainty (Sykes & Menke 2006), which can be addressed only with further geologic and geophysical research.

5. FUTURE RESEARCH DIRECTIONS

Decades of research have led to enviable geologic data sets that record past megathrust earthquakes in Cascadia as well as diverse geophysical observations along the margin. However, major outstanding questions on earthquake occurrence and rupture characteristics remain. In this section, we highlight knowledge gaps, discrepancies between data sets, and uncertainties in earthquake recurrence that may be addressed through collection of new data, careful integration of available data sets, and consideration of the processes that created the records we observe today in Cascadia.

5.1. Outstanding Knowledge Gaps in Cascadia Subduction Zone Earthquake Characteristics and Recurrence

Discrepancies in onshore and offshore geologic evidence for megathrust rupture currently fuel ambiguity in records of megathrust recurrence. Paleoseismic events recorded in the marine record do not all share a corresponding record on land (Figure 4). Mismatch between the data sets is at least partly due to variable evidence thresholds and analytical uncertainties inherent in geochronology (Nelson et al. 2006), but additionally, the geochronologic age corrections applied to onshore and offshore data sets differ, causing difficulty in correlation.

The magnitude of past earthquake events is also difficult to resolve from geologic data sets. Current dating methods and models for CSZ events recorded at individual sites along the margin also have enough uncertainty that experts continue to debate whether full-margin events are always single \sim M9 events or if some small portion might be multiple successive M8 events (Petersen et al. 2014) (Figure 2c). Without Japanese tsunami records and modeling, it is difficult to distinguish the 1700 CE earthquake as a single \sim M9 or multiple \sim M8s. Both paleoseismic and geophysical data sets hint at potentially persistent rupture barriers along the CSZ margin, but it is unclear which barrier proxies are most relevant for understanding coseismic rupture processes. The presence and persistence of rupture barriers may also cause the earthquake cycle model to vary along the megathrust, and the possibility that some past earthquakes were shallow tsunami earthquakes also contributes to uncertainty (Tréhu 2016).

Other aspects of coseismic rupture processes remain elusive. For instance, current geodetic coverage does not uniquely resolve coupling on the subduction zone interface. Without an instrumental record of a great CSZ megathrust earthquake, estimating coseismic onshore and offshore ground motion and secondary hazards, such as liquefaction, landslides, and turbidites, often relies on comparison to other subduction zone margins. The limited liquefaction and landslide evidence for the 1700 CE earthquake inhibits accurately estimating local and regional ground motion for future events. Additionally, numerous assumptions underpin current understanding of shaking-initiated sediment transport processes in the CSZ; we currently lack clarity on how, and under what conditions, the geologic record archives various shaking proxies.

Due to the gaps in knowledge, there is currently no consensus on an appropriate recurrence model for the CSZ. For recurrence estimates, questions remain about the magnitude threshold required to constitute a significant event and whether CSZ geologic records capture all significant earthquakes. Some geologic records may record events less than M8 or record events caused by other earthquake sources, such as the northern San Andreas fault zone (Goldfinger & Gutierrez 2019). Defining a recurrence model and understanding the physical processes influencing recurrence also requires that the geologic record spans enough time to statistically capture potential variability.

5.2. Future Research Directions in Cascadia Subduction Zone Science

Geologic records at the CSZ still present multiple opportunities for advancement. New paleoseismic sites that capitalize on potential for longer temporal records will allow for further exploration of the extent of past megathrust rupture and help identify variability in rupture characteristics. Filling latitudinal spatial gaps in land-level change records may improve recurrence and rupture models (**Supplemental Figure 1**). In addition to study of new locales, modern methodology and statistical analyses can help to reduce uncertainty in available data sets.

New Bayesian transfer functions that can incorporate multiple microfossil proxies reduce uncertainties on subsidence estimates (Kemp et al. 2018), and applying this method downcore can resolve slip over multiple earthquake cycles, improving our knowledge of slip along the megathrust through time and space (Padgett et al. 2021). Microfossil-based analyses also have the potential to quantify interseismic (Shennan et al. 1999) and postseismic (Horton et al. 2017) deformation, but constraining the age of the inorganic tidal mud that accumulates in the postseismic and interseismic periods remains a challenge. At previously investigated locales along the coast (**Supplemental Figure 1**), widespread, precise, quantitative, microfossil-based estimates of coseismic subsidence in 1700 CE have informed heterogeneous rupture models; however, limited and imprecise subsidence estimates for older events do not resolve slip along the megathrust at a high enough resolution to differentiate uniform and heterogeneous model solutions (Leonard et al. 2010, Milker et al. 2016).

Existing uncertainties in dating earthquake events remain one of the largest barriers to reducing the nonuniqueness of geologic correlations and interpretations (Hutchinson & Clague 2017). Dendrochronology offers subannual temporal resolution of land-level changes, and while such resolution still cannot discriminate between serial partial-margin ruptures separated by days or months from single full-margin earthquakes, confidence in the interpretation could improve significantly. Modern dendrochronology methods utilize changes in wood chemistry that may accompany sudden coseismic subsidence (Pearl et al. 2020b) and known spikes in the radiocarbon record as chronologic tie points (Pearl et al. 2020a, Pearson et al. 2020). Dendrochronology could also assist with dating landslide-dammed lakes (Struble et al. 2020). Bayesian age modeling of detrital macrofossil radiocarbon dates provides another promising approach to reduce uncertainties that has been only newly applied in Cascadia (Nelson et al. 2020, Padgett et al. 2021). Offshore, turbidite ages may improve by using more standardized calibrations and reservoir corrections (Clark et al. 2019).

Geodetic models and the near absence of seismicity on the megathrust since the 1700 CE earthquake are consistent with coupling of the CSZ plate boundary to at least some degree (Schmalzle et al. 2014, Wang & Tréhu 2016), but offshore geodetic data are critical for obtaining high-resolution spatial constraints on the degree of coupling and reducing the number of viable coupling models (Bürgmann & Chadwell 2014). Twelve seafloor GNSS-A stations have been deployed on the Juan de Fuca and North American Plates since 1991, most in the past few years. Sites

Supplemental Material >

on the North American Plate near the trench measure shallow coupling (Bürgmann & Chadwell 2014, Heesemann et al. 2017, Chadwell et al. 2018) (**Figure 5**). Researchers plan to deploy at least two more sites on and near the Gorda Plate (**Figure 5**), which features significant internal deformation that is currently poorly constrained (Bartlow 2020). Comparison of the CSZ with other instrumentally monitored subduction zones, such as Nankai (Kano & Kato 2020), can offer clues to the state of coupling, unusual paucity of interplate CSZ seismicity, and the role of slow slip in the accommodation of convergence (Wang & Tréhu 2016, Bartlow 2020).

New structural imaging will also improve definition of potential along-strike rupture boundaries, allowing for better correlations between structure and dynamic behavior of the CSZ. Acquisition of high-resolution offshore imagery and sediment cores across Cascadia's deformation front, combined with quantitative modeling of tsunami generation and sediment transport, will better inform interpretations of tsunami deposits left behind from past earthquakes. Future efforts may also focus on determining whether there is on-fault marine geologic evidence of near-trench rupture along the Cascadia deformation front and the role of splay faults in tsunamigenic rupture (Beeson et al. 2017) (**Figure 1d**).

Broadening the spatial extent of shaking proxy data sets, such as landslides, liquefaction, lacustrine turbidites, and marine turbidites, could substantially improve estimates of past earthquake ground motion. Repeat high-resolution bathymetric mapping and subsurface imaging offer promising techniques to test assumptions made in interpretation of mass-transport deposits (Mountjoy et al. 2018, Hill et al. 2020). Shaking from earthquakes along nonmegathrust crustal faults can complicate interpretation of the geologic record (Clark et al. 2019), although systematic examination of this process along the CSZ has yet to happen and may be an important avenue for future investigation. To this end, lacustrine paleoseismology offers exciting new research avenues to address onshore ground motions for past megathrust events (Morey et al. 2013, Goldfinger et al. 2016), as well as to improve crustal and intraplate earthquake catalogs (van Daele et al. 2019).

5.3. An Integrative Concept for Cascadia Subduction Zone Science

To address and potentially resolve discrepancies and uncertainties in the geologic data, we suggest that future research applies an integrative approach that considers different evidence thresholds of geologic data sets, proxies for megathrust behavior, and potential rupture barriers gleaned from geophysical and instrumental data sets to provide more accurate estimates of past earthquake rupture characteristics.

We can leverage differences in evidence thresholds to learn more about the preservation of earthquake processes in the geologic record. An example from southern Oregon illustrates these thresholds, where Bradley Lake preserves evidence for 12 megathrust-generated tsunami deposits in the past 5,000 years (Kelsey et al. 2005), while nearby subsidence records show only 9 or 10 events in the same time period (Kelsey et al. 2002, Witter et al. 2003). Similarly, while onshore records also suggest a greater number of earthquakes in southern Cascadia (Nelson et al. 2006), not all turbidite events have a corresponding record on land (**Figure 4**). These records may suggest that for some CSZ ruptures, turbidite and/or tsunami deposits are more likely to be created and preserved in southern Cascadia compared to land-level change (Nelson et al. 2006).

Rupture patch location, extent, and slip magnitude likely bear on evidence threshold, as different rupture properties can generate particular secondary effects. For instance, shallow rupture near the trench may cause sufficient seafloor deformation and ground shaking of the accretionary wedge to create tsunamis and turbidites, respectively. The potential for tsunami earthquakes can alter our interpretation of the geologic record and is relevant to consider for structural interpretation. A shallow tsunami earthquake can produce tsunami deposits in a large region indicative of

a M8–9 event but in fact come from a smaller M7–8 event (Hill et al. 2012). Tsunami earthquakes also emit limited high-frequency energy and thus may produce little to no shaking proxies in the geologic record (Newman & Okal 1998, Ye et al. 2016, Sahakian et al. 2019). Integration and careful consideration of the available geologic data sets may therefore enable better mapping of past earthquake extent and estimates of rupture characteristics.

Numerous geophysical data sets provide information about the state of coupling, seismicity, and structure along the CSZ, but interpretations disagree, and models provide nonunique solutions. Systematic and analytical comparisons between geophysical, structural, and modeling data sets both within the CSZ and with other subduction zone margins could assist with better understanding the likelihood of potential rupture barriers and other rupture processes. For example, Wang & Tréhu (2016) note the potential for comparing the offshore morphology and structure of the CSZ accretionary complex to other subduction zone margins that have undergone trench-breaching slip (e.g., 2011 Mw9.0 Tōhoku-Oki event) (Fujiwara et al. 2011).

Inferred relationships between ground motions and shaking-induced sediment transport require rigorous testing, particularly with respect to submarine and terrestrial slope stability, the shear strength of slope sediments, and turbidity flow triggering. New monitoring systems offer in situ observations of shaking and how the sediment structure affects site-specific response to ground motion (Jibson et al. 2004, Gomberg et al. 2019). The distributions of landslides across the landscape in response to ground shaking are often complex and thus difficult to characterize and link to earthquake triggers (LaHusen et al. 2020, Struble et al. 2020). With improved understanding of the relationship between seismic shaking and site properties, there is potential to identify the influence of megathrust earthquake shaking on terrestrial landslides (Meunier et al. 2007, 2013) by comparing landslide catalogs (Jones et al. 2019) with modeled ~M9 seismic ground motions (Frankel et al. 2018, Wirth et al. 2018). Compilation of liquefaction data along the CSZ can also improve shaking estimates in areas with sparse geologic proxies.

The CSZ margin is primed for quantitative and inclusive comparisons of proposed rupture boundaries and characteristics with geologic data sets (**Figures 4 and 5**). Clark et al. (2019) integrated complex and disparate data sets to identify the sources and extents of paleoearthquakes along the Hikurangi margin in New Zealand. Given the extensive geologic data in Cascadia, much of which is more clearly associated with megathrust rupture, a similar approach may be explored along the CSZ. Integration of onshore and offshore geologic records requires uniform treatment of geochronologic data sets, possibly using a Bayesian framework (Clark et al. 2019) that builds upon the recent use and testing of local-scale Bayesian age models (Goldfinger 2014, Nelson et al. 2020, Padgett et al. 2021), as well as identification, and ideally quantification, of evidence thresholds for different record types, with the overarching goal of reducing nonunique fit of past rupture scenarios to the geologic record. The addition of abundant geophysical and instrumental records in Cascadia provides prior knowledge of along-strike heterogeneity that will frame the integration of geologic data sets with constraints from numerical and theoretical modeling (Kemp et al. 2018). A comprehensive catalog of past CSZ megathrust rupture scenarios would provide concrete input for PSHA and may identify specific regions most susceptible to subduction zone earthquakes and associated hazards.

AUTHOR CONTRIBUTIONS

M.A.L.W. and L.M.S. conceived the framework and coordinated the writing of this review. M.A.L.W., L.M.S., and T.D. drafted the initial version of the text with significant contributions and revisions from S.E., J.G., J.K.P., B.S., and A.T. L.M.S. drafted figures. All authors made critical comments and substantive changes throughout the review.

DISCLOSURE STATEMENT

The authors are not aware of any affiliations, memberships, funding, or financial holdings that might be perceived as affecting the objectivity of this review.

ACKNOWLEDGMENTS

This work was conducted as a part of the “Margin-wide geological and geophysical synthesis to understand the recurrence and hazards of great subduction zone earthquakes in Cascadia” project supported by the US Geological Survey John Wesley Powell Center for Analysis and Synthesis. We thank the numerous scientists who contributed to our Powell Center working group meetings and consulted on or reviewed the content of this paper. We especially thank Art Frankel, Alex Grant, Ruth Harris, Charlie Paull, and Richard Styron for their participation in this project, and the Powell Center leadership team, particularly Jill Baron and Leah Colasuonno. Thanks go to Rich Briggs and an anonymous reviewer for their constructive feedback. Any use of trade, product, or firm names is for descriptive purposes only and does not imply endorsement by the US government.

LITERATURE CITED

- Adams J. 1990. Paleoseismicity of the Cascadia Subduction Zone: evidence from turbidites off the Oregon-Washington margin. *Tectonics* 9(4):569–83
- Atwater BF. 1994. *Geology of Holocene liquefaction features along the lower Columbia River at Marsh, Brush, Price, Hunting, and Wallace Islands, Oregon and Washington*. Open File Rep. 94-209, US Geol. Surv., Seattle, WA
- Atwater BF, Carson B, Griggs GB, Johnson HP, Salmi MS. 2014. Rethinking turbidite paleoseismology along the Cascadia subduction zone. *Geology* 42(9):827–30
- Atwater BF, Griggs GB. 2012. *Deep-Sea Turbidites as Guides to Holocene Earthquake History at the Cascadia Subduction Zone: Alternative Views for a Seismic-Hazard Workshop*. Reston, VA: US Geol. Surv.
- Atwater BF, Hemphill-Haley E. 1997. *Recurrence Intervals for Great Earthquakes of the Past 3,500 Years at Northwestern Willapa Bay, Washington*. Washington, DC: US Geol. Surv.
- Atwater BF, Musumi-Rokkaku S, Satake K, Tsuji Y, Ueda K, Yamaguchi DK. 2005. *The Orphan Tsunami of 1700*. Seattle: Univ. Washington Press
- Atwater BF, Yamaguchi DK. 1991. Sudden, probably coseismic submergence of Holocene trees and grass in coastal Washington State. *Geology* 19(7):706–9
- Bartlow NM. 2020. A long-term view of episodic tremor and slip in Cascadia. *Geophys. Res. Lett.* 47(3):e2019GL085303
- Bartlow NM, Miyazaki S, Bradley AM, Segall P. 2011. Space-time correlation of slip and tremor during the 2009 Cascadia slow slip event. *Geophys. Res. Lett.* 38(18):L18309
- Bassett D, Sandwell DT, Fialko Y, Watts AB. 2016. Upper-plate controls on co-seismic slip in the 2011 magnitude 9.0 Tohoku-oki earthquake. *Nature* 531(7592):92–96
- Beeler NM, Roeloffs E, McCausland W. 2014. Re-estimated effects of deep episodic slip on the occurrence and probability of great earthquakes in Cascadia. *Bull. Seismol. Soc. Am.* 104(1):128–44
- Beeson JW, Goldfinger C, Fortin WF. 2017. Large-scale modification of submarine geomorphic features on the Cascadia accretionary wedge caused by catastrophic flooding events. *Geosphere* 13(5):1713–28
- Bilek SL, Lay T. 2018. Subduction zone megathrust earthquakes. *Geosphere* 14(4):1468–500
- Blais-Stevens A, Rogers GC, Clague JJ. 2011. A revised earthquake chronology for the last 4,000 years inferred from varve-bounded debris-flow deposits beneath an inlet near Victoria, British Columbia. *Bull. Seismol. Soc. Am.* 101(1):1–12
- Bodmer M, Toomey DR, Hoofft EEE, Schmandt B. 2018. Buoyant asthenosphere beneath Cascadia influences megathrust segmentation. *Geophys. Res. Lett.* 45(14):6954–62
- Boyarko DC, Brudzinski MR, Porritt RW, Allen RM, Tréhu AM. 2015. Automated detection and location of tectonic tremor along the entire Cascadia margin from 2005 to 2011. *Earth Planet. Sci. Lett.* 430:160–70

- Brudzinski MR, Allen RM. 2007. Segmentation in episodic tremor and slip all along Cascadia. *Geology* 35(10):907–10
- Bruhat L, Segall P. 2016. Coupling on the northern Cascadia subduction zone from geodetic measurements and physics-based models. *J. Geophys. Res. Solid Earth* 121(11):8297–314
- Bürgmann R, Chadwell D. 2014. Seafloor geodesy. *Annu. Rev. Earth Planet. Sci.* 42:509–34
- Chadwell CD, Schmidt DA, Webb SC, Nooner SL, Erickson TL, et al. 2018. *Expansion of GPS-acoustic arrays offshore the Cascadia and Alaska subduction zones*. Presented at AGU Fall Meet., Dec. 10–14, Washington, DC, Abstr. T44C-02
- Clague JJ, Bobrowsky PT, Hutchinson I. 2000. A review of geological records of large tsunamis at Vancouver Island, British Columbia, and implications for hazard. *Quat. Sci. Rev.* 19(9):849–63
- Clark K, Howarth J, Litchfield N, Cochran U, Turnbull J, et al. 2019. Geological evidence for past large earthquakes and tsunamis along the Hikurangi subduction margin, New Zealand. *Mar. Geol.* 412:139–72
- Cornell CA. 1968. Engineering seismic risk analysis. *Bull. Seismol. Soc. Am.* 58(5):1583–606
- Cornell CA, Winterstein SR. 1988. Temporal and magnitude dependence in earthquake recurrence models. *Bull. Seismol. Soc. Am.* 78(4):1522–37
- Cramer CH, Petersen MD, Cao T, Topozada TR, Reichle M. 2000. A time-dependent probabilistic seismic-hazard model for California. *Bull. Seismol. Soc. Am.* 90(1):1–21
- Cubas N, Avouac JP, Souloumiac P, Leroy Y. 2013. Megathrust friction determined from mechanical analysis of the forearc in the Maule earthquake area. *Earth Planet. Sci. Lett.* 381:92–103
- Darlenzo ME, Peterson CD, Clough C. 1994. Stratigraphic evidence for great subduction-zone earthquakes at four estuaries in northern Oregon, USA. *J. Coast. Res.* 10(4):850–76
- Davis D, Dahlen FA, Suppe J. 1983. Mechanics of fold-and-thrust belts and accretionary wedges cohesive Coulomb theory. *J. Geophys. Res.* 88(B2):1153–72
- Dragert H, Wang K, James TS. 2001. A silent slip event on the deeper Cascadia subduction interface. *Science* 292(5521):1525–28
- Dura T, Engelhart SE, Vacchi M, Horton BP, Kopp RE, et al. 2016a. The role of Holocene relative sea-level change in preserving records of subduction zone earthquakes. *Curr. Clim. Change Rep.* 2(3):86–100
- Dura T, Hemphill-Haley E, Sawai Y, Horton BP. 2016b. The application of diatoms to reconstruct the history of subduction zone earthquakes and tsunamis. *Earth-Sci. Rev.* 152:181–97
- Engelhart SE, Vacchi M, Horton BP, Nelson AR, Kopp RE. 2015. A sea-level database for the Pacific coast of central North America. *Quat. Sci. Rev.* 113:78–92
- Enkin RJ, Dallimore A, Baker J, Southon JR, Ivanochko T. 2013. A new high-resolution radiocarbon Bayesian age model of the Holocene and Late Pleistocene from core MD02–2494 and others, Effingham Inlet, British Columbia, Canada; with an application to the paleoseismic event chronology of the Cascadia Subduction Zone. *Can. J. Earth Sci.* 50(7):746–60
- Espinosa AF. 1976. *The Guatemalan earthquake of February 4, 1976*. Prof. Pap. 1002., US Geol. Surv. Washington, DC
- Field EH. 2015. Computing elastic-rebound-motivated earthquake probabilities in unsegmented fault models: a new methodology supported by physics-based simulators. *Bull. Seismol. Soc. Am.* 105(2):544–59
- Frankel A. 2013. Rupture history of the 2011 M 9 Tohoku Japan earthquake determined from strong-motion and high-rate GPS recordings: subevents radiating energy in different frequency bands. *Bull. Seismol. Soc. Am.* 103(2B):1290–306
- Frankel A, Chen R, Petersen M, Moschetti M, Sherrod B. 2015. 2014 Update of the Pacific Northwest portion of the U.S. National Seismic Hazard Maps. *Earthq. Spectra* 31(S1):S131–48
- Frankel A, Wirth E, Marafi N, Vidale J, Stephenson W. 2018. Broadband synthetic seismograms for magnitude 9 earthquakes on the Cascadia megathrust based on 3D simulations and stochastic synthetics, part 1: methodology and overall results. *Bull. Seismol. Soc. Am.* 108(5A):2347–69
- Fujie G, Kodaira S, Yamashita M, Sato T, Takahashi T, Takahashi N. 2013. Systematic changes in the incoming plate structure at the Kuril trench. *Geophys. Res. Lett.* 40(1):88–93
- Fujiwara T, Kodaira S, No T, Kaiho Y, Takahashi N, Kaneda Y. 2011. The 2011 Tohoku-Oki earthquake: displacement reaching the trench axis. *Science* 334(6060):1240
- Gao X, Wang K. 2017. Rheological separation of the megathrust seismogenic zone and episodic tremor and slip. *Nature* 543(7645):416–19

- Garrett E, Fujiwara O, Garrett P, Heyvaert VMA, Shishikura M, et al. 2016. A systematic review of geological evidence for Holocene earthquakes and tsunamis along the Nankai-Suruga Trough, Japan. *Earth-Sci. Rev.* 159:337–57
- Garrison-Laney C, Miller I. 2017. Tsunamis in the Salish Sea: recurrence, sources, hazards. *GSA Field Guide* 49:67–78
- Gavey R, Carter L, Liu JT, Talling PJ, Hsu R, et al. 2017. Frequent sediment density flows during 2006 to 2015, triggered by competing seismic and weather events: observations from subsea cable breaks off southern Taiwan. *Mar. Geol.* 384:147–58
- Geist EL. 2002. Complex earthquake rupture and local tsunamis. *J. Geophys. Res.* 107(B5):ESE 2-1–2-15
- Geist EL. 2005. Rapid tsunami models and earthquake source parameters: far-field and local applications. *ISET J. Earthq. Technol.* 42(4):127–36
- Goff J, Bobrowsky P, Huntley D, Sawai Y, Tanagawa K. 2020. Palaeotsunamis along Canada's Pacific coast. *Quat. Sci. Rev.* 237:106309
- Goldfinger C. 2014. Integrating onshore and offshore paleoseismic data: a Bayesian model. *Geol. Soc. Am. Abstr. Programs* 46. <https://doi.org/10.13140/2.1.3738.4967>
- Goldfinger C, Galer S, Beeson J, Hamilton T, Black B, et al. 2017. The importance of site selection, sediment supply, and hydrodynamics: a case study of submarine paleoseismology on the northern Cascadia margin, Washington USA. *Mar. Geol.* 384:4–46
- Goldfinger C, Gutierrez J. 2019. *Possible stratigraphic evidence of stress triggering of the Northern San Andreas Fault following Southern Cascadia earthquakes*. Presented at AGU Fall Meet., Dec. 9–13, San Francisco, Abstr. OS54A-03
- Goldfinger C, Ikeda Y, Yeats RS, Ren J. 2013a. Superquakes and supercycles. *Seismol. Res. Lett.* 84(1):24–32
- Goldfinger C, Kulm LD, McNeill LC, Watts P. 2000. Super-scale failure of the southern Oregon Cascadia margin. *Pure Appl. Geophys.* 157(6–8):1189–226
- Goldfinger C, Morey AE, Black B, Beeson J, Nelson CH, et al. 2013b. Spatially limited mud turbidites on the Cascadia margin: segmented earthquake ruptures? *Nat. Hazard Earth Syst. Sci.* 13(8):2109–46
- Goldfinger C, Nelson CH, Morey AE, Johnson JE, Patton JR, et al. 2012. *Turbidite event history—methods and implications for Holocene paleoseismicity of the Cascadia subduction zone*. Prof. Pap. 1661-F, US Geol. Surv., Washington, DC
- Goldfinger C, Wong I, Kulkarni R, Beeson JW. 2016. Reply to “Comment on ‘Statistical analyses of great earthquake recurrence along the Cascadia subduction zone.’” *Bull. Seismol. Soc. Am.* 106(6):2935–44
- Gomberg J. 2010. Slow-slip phenomena in Cascadia from 2007 and beyond: a review. *GSA Bull.* 122(7–8):963–78
- Gomberg J, Hautala S, Johnson P, Chiswell S. 2019. Separating sea and slow slip signals on the seafloor. *J. Geophys. Res. Solid Earth* 124(12):13486–503
- Gomberg J, Ludwig KA, Bekins B, Brocher TM, Brock JC, et al. 2017. *Reducing Risk Where Tectonic Plates Collide—U.S. Geological Survey Subduction Zone Science Plan*. Reston, VA: US Geol. Surv.
- Hamilton TS, Enkin RJ, Riedel M, Rogers GC, Pohlman JW, et al. 2015. Slipstream: an early Holocene slump and turbidite record from the frontal ridge of the Cascadia accretionary wedge off western Canada and paleoseismic implications. *Can. J. Earth Sci.* 52(6):405–30
- Hansen WR. 1965. *Effects of the Earthquake of March 27, 1964, at Anchorage, Alaska*. Washington, DC: US GPO
- Hawkes AD, Horton BP, Nelson AR, Vane CH, Sawai Y. 2011. Coastal subsidence in Oregon, USA, during the giant Cascadia earthquake of AD 1700. *Quat. Sci. Rev.* 30(3–4):364–76
- Heesemann M, Wang K, Davis E, Chadwell CD, Nissen E, et al. 2017. *Plans for a northern Cascadia subduction zone observatory*. Presented at AGU Fall Meet., Dec. 11–15, New Orleans, Abstr. T51E-1287
- Hemphill-Haley E. 1995. Diatom evidence for earthquake-induced subsidence and tsunami 300 yr ago in southern coastal Washington. *GSA Bull.* 107(3):367–78
- Henstock TJ, McNeill LC, Bull JM, Cook BJ, Gulick SPS, et al. 2016. Downgoing plate topography stopped rupture in the A.D. 2005 Sumatra earthquake. *Geology* 44(1):71–74
- Herrendörfer R, Van Dinther Y, Gerya T, Dalguer LA. 2015. Earthquake supercycle in subduction zones controlled by the width of the seismogenic zone. *Nat. Geosci.* 8(6):471–74

- Hill EM, Borrero JC, Huang Z, Qiu Q, Banerjee P, et al. 2012. The 2010 Mw 7.8 Mentawai earthquake: Very shallow source of a rare tsunami earthquake determined from tsunami field survey and near-field GPS data. *J. Geophys. Res.* 117(B6):B06402
- Hill JC, Watt JT, Brothers DS, Kluesner JW. 2020. Submarine canyons, slope failures and mass transport processes in southern Cascadia. *Geol. Soc. Lond. Spec. Publ.* 500:453–475
- Horton BP, Milker Y, Dura T, Wang K, Bridgeland WT, et al. 2017. Microfossil measures of rapid sea-level rise: timing of response of two microfossil groups to a sudden tidal-flooding experiment in Cascadia. *Geology* 45(6):535–38
- Howarth J, Orpin AR, Nodder S, McCleery D, Strachan LJ, et al. 2018. *Calibrating the turbidite paleoseismometer on the Hikurangi margin, New Zealand, using the 2016 Mw7.8 Kaikoura earthquake*. Presented at AGU Fall Meet., Dec. 10–14, Washington, DC, Abstr. T53C-01
- Hutchinson I. 1992. *Holocene Sea Level Change in the Pacific Northwest: A Catalogue of Radiocarbon Dates and an Atlas of Regional Sea-Level Curves*. Burnaby, Can.: Inst. Quat. Res.
- Hutchinson I, Clague J. 2017. Were they all giants? Perspectives on late Holocene plate-boundary earthquakes at the northern end of the Cascadia subduction zone. *Quat. Sci. Rev.* 169:29–49
- Hyndman RD, McCrory PA, Wech A, Kao H, Ague J. 2015. Cascadia subducting plate fluids channelled to fore-arc mantle corner: ETS and silica deposition. *J. Geophys. Res. Solid Earth* 120(6):4344–58
- Jacoby G, Bunker DE, Benson BE. 1997. Tree-ring evidence for an A.D. 1700 Cascadia earthquake in Washington and northern Oregon. *Geology* 25(11):999–1002
- Jacoby G, Carver G, Wagner W. 1995. Trees and herbs killed by an earthquake ~300 yr ago at Humboldt Bay, California. *Geology* 23(1):77–80
- Jibson RW, Harp EL, Schulz W, Keefer DK. 2004. Landslides triggered by the 2002 Denali Fault, Alaska, earthquake and the inferred nature of the strong shaking. *Earthq. Spectra* 20(3):669–91
- Jones ES, Mirus BB, Schmitt RG, Baum RL, Burns WJ, et al. 2019. *Landslide inventories across the United States*. U.S. Geological Survey Data Release, US Geol. Surv., Washington, DC, updated March 9. <https://doi.org/10.5066/P9E2A37P>
- Kano M, Kato A. 2020. Detailed spatial slip distribution for short-term slow slip events along the Nankai subduction zone, southwest Japan. *J. Geophys. Res. Solid Earth* 125:e2020JB019613
- Karlin RE, Holmes M, Abella SEB, Sylwester R. 2004. Holocene landslides and a 3500-year record of Pacific Northwest earthquakes from sediments in Lake Washington. *GSA Bull.* 116(1–2):94–108
- Kelsey HM, Nelson AR, Hemphill-Haley E, Witter RC. 2005. Tsunami history of an Oregon coastal lake reveals a 4600 yr record of great earthquakes on the Cascadia subduction zone. *GSA Bull.* 117(7–8):1009–32
- Kelsey HM, Witter RC, Hemphill-Haley E. 2002. Plate-boundary earthquakes and tsunamis of the past 5500 yr, Sixes River estuary, southern Oregon. *GSA Bull.* 114(3):298–314
- Kemp AC, Cahill N, Engelhart SE, Hawkes AD, Wang K. 2018. Revising estimates of spatially variable subsidence during the A.D. 1700 Cascadia earthquake using a Bayesian foraminiferal transfer function. *Bull. Seismol. Soc. Am.* 108(2):654–73
- Kirk R. 2015. *Ozette: Excavating a Makah Whaling Village*. Seattle: Univ. Washington Press
- Kulkarni R, Wong I, Zachariassen J, Goldfinger C, Lawrence M. 2013. Statistical analyses of great earthquake recurrence along the Cascadia subduction zone. *Bull. Seismol. Soc. Am.* 103(6):3205–21
- LaHusen SR, Duvall AR, Booth AM, Grant A, Mishkin BA, et al. 2020. Rainfall triggers more deep-seated landslides than Cascadia earthquakes in the Oregon Coast Range, USA. *Sci. Adv.* 6(38):eaba6790
- Lamb S. 2006. Shear stresses on megathrusts: implications for mountain building behind subduction zones. *J. Geophys. Res.* 111(B7):B07401
- Lay T, Kanamori H, Ammon CJ, Koper KD, Hutko AR, et al. 2012. Depth-varying rupture properties of subduction zone megathrust faults. *J. Geophys. Res.* 117(4):B04311
- Leithold EL, Wegmann KW, Bohnenstiehl DR, Joyner CN, Pollen AF. 2019. Repeated megaturbidite deposition in Lake Crescent, Washington, USA, triggered by Holocene ruptures of the Lake Creek-Boundary Creek fault system. *GSA Bull.* 131(11–12):2039–55
- Leithold EL, Wegmann KW, Bohnenstiehl DR, Smith SG, Noren A, O’Grady R. 2018. Slope failures within and upstream of Lake Quinalt, Washington, as uneven responses to Holocene earthquakes along the Cascadia subduction zone. *Quat. Res.* 89(1):178–200

- Leonard LJ, Currie CA, Mazzotti S, Hyndman RD. 2010. Rupture area and displacement of past Cascadia great earthquakes from coastal coseismic subsidence. *GSA Bull.* 122(11–12):2079–96
- Leonard LJ, Hyndman RD, Mazzotti S. 2004. Coseismic subsidence in the 1700 great Cascadia earthquake: coastal estimates versus elastic dislocation models. *GSA Bull.* 116(5–6):655–70
- Li D, Liu Y. 2016. Modeling slow-slip segmentation in Cascadia subduction zone constrained by tremor locations and gravity anomalies. *J. Geophys. Res. Solid Earth* 122(4):3138–57
- Li S, Wang K, Wang Y, Jiang Y, Dosso SE. 2018. Geodetically inferred locking state of the Cascadia megathrust based on a viscoelastic Earth model. *J. Geophys. Res. Solid Earth* 123:8056–72
- Long AJ, Shennan I. 1998. Models of rapid relative sea-level change in Washington and Oregon, USA. *Holocene* 8(2):129–42
- Mazzotti S, Adams J. 2004. Variability of near-term probability for the next great earthquake on the Cascadia subduction zone. *Bull. Seismol. Soc. Am.* 94(5):1954–59
- McCaffrey R, King RW, Payne SJ, Lancaster M. 2013. Active tectonics of northwestern U.S. inferred from GPS-derived surface velocities. *J. Geophys. Res. Solid Earth* 118(2):709–23
- McCrorry PA, Blair JL, Waldhauser F, Oppenheimer DH. 2012. Juan de Fuca slab geometry and its relation to Wadati-Benioff zone seismicity. *J. Geophys. Res. Solid Earth* 117(B9):B09306
- McGuire JJ, Plank T, Barrientos S, Becker T, Brodsky E, Cottrell E. 2017. *The SZAD Initiative: Understanding the Processes That Underlie Subduction Zone Hazards in 4D*. Washington, DC: IRIS Consort.
- McNeill LC, Henstock TJ. 2014. Forearc structure and morphology along the Sumatra-Andaman subduction zone. *Tectonics* 33(2):112–34
- Melgar D, Leveque RJ, Dreger DS, Allen RM. 2016. Kinematic rupture scenarios and synthetic displacement data: an example application to the Cascadia subduction zone. *J. Geophys. Res. Solid Earth* 121:6658–74
- Meltzner AJ, Sieh K, Chiang H-W, Shen C-C, Suwargadi BW, et al. 2012. Persistent termini of 2004- and 2005-like ruptures of the Sunda megathrust. *J. Geophys. Res.* 117(B4):B04405
- Meunier P, Hovius N, Haines AJ. 2007. Regional patterns of earthquake-triggered landslides and their relation to ground motion. *Geophys. Res. Lett.* 34(20):L20408
- Meunier P, Uchida T, Hovius N. 2013. Landslide patterns reveal the sources of large earthquakes. *Earth Planet. Sci. Lett.* 363:27–33
- Michel S, Gualandi A, Avouac JP. 2018. Interseismic coupling and slow slip events on the Cascadia megathrust. *Pure Appl. Geophys.* 176:3867–91
- Milker Y, Nelson AR, Horton BP, Engelhart SE, Bradley LA, et al. 2016. Differences in coastal subsidence in southern Oregon (USA) during at least six prehistoric megathrust earthquakes. *Quat. Sci. Rev.* 142:143–63
- Moernaut J, van Daele M, Fontijn K, Heirman K, Kempf P, et al. 2018. Larger earthquakes recur more periodically: new insights in the megathrust earthquake cycle from lacustrine turbidite records in south-central Chile. *Earth Planet. Sci. Lett.* 481:9–19
- Morey AE, Goldfinger C, Briles CE, Gavin DG, Colombaroli D, Kusler JE. 2013. Are great Cascadia earthquakes recorded in the sedimentary records from small forearc lakes? *Nat. Hazards Earth Syst. Sci.* 13(10):2441–63
- Morton EA, Bilek SL, Rowe CA. 2018. Newly detected earthquakes in the Cascadia subduction zone linked to seamount subduction and deformed upper plate. *Geology* 46(11):943–46
- Mountjoy JJ, Howarth JD, Orpin AR, Barnes PM, Bowden DA, et al. 2018. Earthquakes drive large-scale submarine canyon development and sediment supply to deep-ocean basins. *Sci. Adv.* 4(3):eaar3748
- Nelson AR, Atwater BF, Bobrowsky PT, Bradley L-A, Clague JJ, et al. 1995. Radiocarbon evidence for extensive plate-boundary rupture about 300 years ago at the Cascadia subduction zone. *Nature* 378(6555):371–74
- Nelson AR, Hawkes AD, Sawai Y, Engelhart SE, Witter R, et al. 2020. Identifying the greatest earthquakes of the past 2000 years at the Nehalem river Estuary, northern Oregon coast, USA. *Open Quat.* 6(2):1–30
- Nelson AR, Hawkes AD, Sawai Y, Horton BP, Witter RC, et al. 2021. Minimal stratigraphic evidence for coseismic coastal subsidence during 2000 yr of megathrust earthquakes at the central Cascadia subduction zone. *Geosphere* 17:171–200
- Nelson AR, Kelsey HM, Witter RC. 2006. Great earthquakes of variable magnitude at the Cascadia subduction zone. *Quat. Res.* 65(3):354–65

- Nelson AR, Sawai Y, Jennings AE, Bradley LA, Gerson L, et al. 2008. Great-earthquake paleogeodesy and tsunamis of the past 2000 years at Alsea Bay, central Oregon coast, USA. *Quat. Sci. Rev.* 27(7–8):747–68
- Nelson AR, Shennan I, Long AJ. 1996. Identifying coseismic subsidence in tidal-wetland stratigraphic sequences at the Cascadia subduction zone of western North America. *J. Geophys. Res.* 101(B3):6115–35
- Newman AV, Okal EA. 1998. Teleseismic estimates of radiated seismic energy: The *E/M0* discriminant for tsunami earthquakes. *J. Geophys. Res.* 103(B11):26885–98
- Nocquet JM, Jarrin P, Vallée M, Mothes PA, Grandin R, et al. 2017. Supercycle at the Ecuadorian subduction zone revealed after the 2016 Pedernales earthquake. *Nat. Geosci.* 10(2):145–49
- Obara K, Kato A. 2016. Connecting slow earthquakes to huge earthquakes. *Science* 353(6296):253–57
- Obermeier SF. 1995. *Preliminary estimates of the strength of prehistoric shaking in the Columbia River Valley and the southern half of coastal Washington, with emphasis for a Cascadia subduction zone earthquake about 300 years ago*. Open File Rep. 94–589, US Geol. Surv., Seattle, WA
- Obermeier SF, Atwater BF, Benson BE, Peterson CD, Moses LJ, et al. 1993. Liquefaction about 300 years ago along tidal marshes of the Columbia River, Oregon and Washington. *Eos Trans. AGU* 74:198
- Obermeier SF, Dickenson SE. 2000. Liquefaction evidence for the strength of ground motions resulting from late Holocene Cascadia subduction earthquakes, with emphasis on the event of 1700 A.D. *Bull. Seismol. Soc. Am.* 90(4):876–96
- Olsen KM, Bangs NL, Tréhu AM, Han S, Arnulf A, Contreras-Reyes E. 2020. Thick, strong sediment subduction along south-central Chile and its role in great earthquakes. *Earth Planet. Sci. Lett.* 538:116195
- Padgett JS, Engelhart SE, Kelsey HM, Witter RC, Cahill N, Hemphill-Haley E. 2021. Timing and amount of southern Cascadia earthquake subsidence over the past 1700 years at northern Humboldt Bay, California, USA. *GSA Bull.* <https://doi.org/10.1130/B35701.1>
- Pearl JK, Anchukaitis KJ, Donnelly JP, Pearson C, Pederson N, et al. 2020a. A late Holocene subfossil Atlantic white cedar tree-ring chronology from the northeastern United States. *Quat. Sci. Rev.* 228:106104
- Pearl JK, Keck JR, Tintor W, Siekacz L, Herrick HM, et al. 2020b. New frontiers in tree-ring research. *Holocene* 30(6):923–41
- Pearson C, Salzer M, Wacker L, Brewer P, Sookdeo A, Kuniholm P. 2020. Securing timelines in the ancient Mediterranean using multiproxy annual tree-ring data. *PNAS* 117(15):8410–15
- Perkins JP, Roering JJ, Burns WJ, Strubel W, Black BA, et al. 2018. Hunting for landslides from Cascadia's great earthquakes. *Eos Trans. AGU* 99:2018EO103689
- Peters R, Jaffe B, Gelfenbaum G. 2007. Distribution and sedimentary characteristics of tsunami deposits along the Cascadia margin of western North America. *Sediment. Geol.* 200:372–86
- Petersen MD, Cramer CH, Frankel AD. 2002. Simulations of seismic hazard for the Pacific Northwest of the United States from earthquakes associated with the Cascadia subduction zone. *Pure Appl. Geophys.* 159(9):2147–68
- Petersen MD, Moschetti MP, Powers PM, Mueller CS, Haller KM, et al. 2014. *Documentation for the 2014 update of the United States National Seismic Hazard Maps*. Open File Rep. 2014-1091, US Geol. Surv., Seattle, WA
- Petersen MD, Shumway AM, Powers PM, Mueller CS, Moschetti MP, et al. 2019. The 2018 update of the US National Seismic Hazard Model: overview of model and implications. *Earthq. Spectra* 36(1):5–41
- Peterson CD, Carver GA, Cruikshank KM, Abramson HF, Garrison-Laney CE, et al. 2011. Evaluation of the use of paleotsunami deposits to reconstruct inundation distance and runup heights associated with prehistoric inundation events, Crescent City, southern Cascadia margin. *Earth Surf. Proc. Landf.* 36(7):967–80
- Philibosian B, Meltzner AJ. 2020. Segmentation and supercycles: a catalog of earthquake rupture patterns from the Sumatran Sunda Megathrust and other well-studied faults worldwide. *Quat. Sci. Rev.* 241:106390
- Pollitz FF, Evans EL. 2017. Implications of the earthquake cycle for inferring fault locking on the Cascadia megathrust. *Geophys. J. Int.* 209(1):167–85
- Porritt RW, Allen RM, Boyarko DC, Brudzinski MR. 2011. Investigation of Cascadia segmentation with ambient noise tomography. *Earth Planet. Sci. Lett.* 309(1):67–76
- Praet N, Moernaut J, van Daele M, Boes E, Haeussler PJ, et al. 2017. Paleoseismic potential of sublacustrine landslide records in a high-seismicity setting (south-central Alaska). *Mar. Geol.* 384:103–19

- Priest GR, Zhang Y, Witter RC, Wang K, Goldfinger C, Stimely L. 2014. Tsunami impact to Washington and northern Oregon from segment ruptures on the southern Cascadia subduction zone. *Nat. Hazards* 72(2):849–70
- Reid HF. 1910. *The mechanics of the earthquake, in the California earthquake of 18 April 1906*. Rep. State Earthq. Investig. Comm., Carnegie Inst., Washington, DC
- Rogers G, Dragert H. 2003. Episodic tremor and slip on the Cascadia subduction zone: the chatter of silent slip. *Science* 300(5627):1942–43
- Rong Y, Jackson DD, Magistrale H, Goldfinger C. 2014. Magnitude limits of subduction zone earthquakes. *Bull. Seismol. Soc. Am.* 104(5):2359–77
- Roten D, Olsen KB, Takedatsu R. 2019. Numerical simulation of M9 megathrust earthquakes in the Cascadia subduction zone. *Pure Appl. Geophys.* 177(2020):2125–41
- Saffer DM, Bekins BA. 2002. Hydrologic controls on the morphology and mechanics of accretionary wedges. *Geology* 30(3):271–74
- Sahakian VJ, Melgar D, Muzli M. 2019. Weak near-field behavior of a tsunami earthquake: toward real-time identification for local warning. *Geophys. Res. Lett.* 46(16):9519–28
- Saillard M, Audin L, Rousset B, Avouac JP, Chlieh M, et al. 2017. From the seismic cycle to long-term deformation: linking seismic coupling and Quaternary coastal geomorphology along the Andean megathrust. *Tectonics* 36(2):241–56
- Satake K, Wang K, Atwater BF. 2003. Fault slip and seismic moment of the 1700 Cascadia earthquake inferred from Japanese tsunami descriptions. *J. Geophys. Res.* 108(B11):2535
- Schmalzle GM, McCaffrey R, Creager KC. 2014. Central Cascadia subduction zone creep. *Geochem. Geophys. Geosyst.* 15(4):1515–32
- Scholz CH. 2014. Holocene earthquake history of Cascadia: a quantitative test. *Bull. Seismol. Soc. Am.* 104(4):2120–24
- Schulz WH, Galloway SL, Higgins JD. 2012. Evidence for earthquake triggering of large landslides in coastal Oregon, USA. *Geomorphology* 141:88–98
- Schwartz DP, Coppersmith KJ. 1984. Fault behavior and characteristic earthquakes: examples from the Wasatch and San Andreas Fault Zones. *J. Geophys. Res.* 89(B7):5681–98
- Shennan I, Garrett E, Barlow N. 2016. Detection limits of tidal-wetland sequences to identify variable rupture modes of megathrust earthquakes. *Quat. Sci. Rev.* 150:1–30
- Shennan I, Long AJ, Rutherford MM, Green FM, Innes JB, et al. 1996. Tidal marsh stratigraphy, sea-level change and large earthquakes, I: a 5000 year record in Washington, U.S.A. *Quat. Sci. Rev.* 15(10):1023–59
- Shennan I, Scott DB, Rutherford M, Zong Y. 1999. Microfossil analysis of sediments representing the 1964 earthquake, exposed at Girdwood Flats, Alaska, USA. *Quat. Int.* 60(1):55–73
- Shimazaki K, Nakata T. 1980. Time-predictable recurrence model for large earthquakes. *Geophys. Res. Lett.* 7(4):279–82
- Sieh K, Natawidjaja DH, Meltzner AJ, Shen CC, Cheng H, et al. 2008. Earthquake supercycles inferred from sea-level changes recorded in the corals of west Sumatra. *Science* 322(5908):1674–78
- Stone I, Vidale JE, Han S, Roland E. 2018. Catalog of offshore seismicity in Cascadia: insights into the regional distribution of microseismicity and its relation to subduction processes. *J. Geophys. Res. Solid Earth* 123(1):641–52
- Struble WT, Roering JJ, Black BA, Burns WJ, Calhoun N, Wetherell L. 2020. Dendrochronological dating of landslides in western Oregon: searching for signals of the Cascadia AD 1700 earthquake. *GSA Bull.* 132(7–8):1775–91
- Sykes LR, Menke W. 2006. Repeat times of large earthquakes: implications for earthquake mechanics and long-term prediction. *Bull. Seismol. Soc. Am.* 96(5):1569–96
- Takada K, Atwater BF. 2004. Evidence for liquefaction identified in peeled slices of Holocene deposits along the Lower Columbia River, Washington. *Bull. Seismol. Soc. Am.* 94(2):550–75
- Tréhu AM. 2016. Source parameter scaling and the Cascadia paleoseismic record. *Bull. Seismol. Soc. Am.* 106(3):904–11
- Tréhu AM, Asudeh I, Brocher TM, Luetgert JH, Mooney WD, et al. 1994. Crustal architecture of the Cascadia forearc. *Science* 266(5183):237–43

- Tréhu AM, Blakely RJ, Williams MC. 2012. Subducted seamounts and recent earthquakes beneath the central Cascadia forearc. *Geology* 40(2):103–6
- Tréhu AM, Braunmiller J, Davis E. 2015. Seismicity of the central Cascadia continental margin near 44.5° N: a decadal view. *Seismol. Res. Lett.* 86(3):819–29
- Tréhu AM, Hass B, de Moor A, Maksymowicz A, Contreras-Reyes E, et al. 2019. Geologic controls on up-dip and along-strike propagation of slip during subduction zone earthquakes from a high-resolution seismic reflection survey across the northern limit of slip during the 2010 M_w 8.8 Maule earthquake, offshore Chile. *Geosphere* 15(6):1751–73
- van Daele M, Araya-Cornejo C, Pille T, Vanneste K, Moernaut J, et al. 2019. Distinguishing intraplate from megathrust earthquakes using lacustrine turbidites. *Geology* 47(2):127–30
- Vandekerckhove E, van Daele M, Praet N, Cnudde V, Haeussler PJ, et al. 2020. Flood-triggered versus earthquake-triggered turbidites: a sedimentological study in clastic lake sediments (Eklutna Lake, Alaska). *Sedimentology* 67(1):364–89
- Veblen TT, Ashton DH. 1978. Catastrophic influences on the vegetation of the Valdivian Andes, Chile. *Vegetation* 36(3):149–67
- Victor P, Sobiesiak M, Glodny J, Nielsen SN, Oncken O. 2011. Long-term persistence of subduction earthquake segment boundaries: evidence from Mejillones Peninsula, northern Chile. *J. Geophys. Res.* 116(B2):B0240
- von Huene R, Scholl DW. 1991. Observations at convergent margins concerning sediment subduction, subduction erosion, and the growth of continental crust. *Rev. Geophys.* 29(3):279–316
- Wang D, Mori J. 2011. Frequency-dependent energy radiation and fault coupling for the 2010 M_w 8.8 Maule, Chile, and 2011 M_w 9.0 Tohoku, Japan, earthquakes. *Geophys. Res. Lett.* 38(22):L22308
- Wang K, Tréhu AM. 2016. Invited review paper: some outstanding issues in the study of great megathrust earthquakes—the Cascadia example. *J. Geodyn.* 98:1–18
- Wang K, Wells R, Mazzotti S, Hyndman RD, Sagiya T. 2003. A revised dislocation model of interseismic deformation of the Cascadia subduction zone. *J. Geophys. Res.* 108(B1):2026
- Wang PL, Engelhart SE, Wang K, Hawkes AD, Horton BP, et al. 2013. Heterogeneous rupture in the great Cascadia earthquake of 1700 inferred from coastal subsidence estimates. *J. Geophys. Res. Solid Earth* 118(5):2460–73
- Wartman J, Dunham L, Tiwari B, Pradel D. 2013. Landslides in eastern Honshu induced by the 2011 Tohoku earthquake. *Bull. Seismol. Soc. Am.* 103(2B):1503–21
- Watt JT, Brothers DS. 2021. Systematic characterization of morpho-tectonic variability along the Cascadia convergent margin: implications for shallow megathrust behavior and hazards. *Geosphere* 17:95–117
- Wells RE, Blakely RJ, Sugiyama Y, Scholl DW, Dinterman PA. 2003. Basin-centered asperities in great subduction zone earthquakes: a link between slip, subsidence, and subduction erosion? *J. Geophys. Res.* 108(B10):2507
- Wells RE, Blakely RJ, Wech AG, McCrory PA, Michael A. 2017. Cascadia subduction tremor muted by crustal faults. *Geology* 45(6):515–18
- Wells RE, Weaver CS, Blakely RJ. 1998. Fore-arc migration in Cascadia and its neotectonic significance. *Geology* 26(8):759–62
- Williams HF, Hutchinson I, Nelson AR. 2005. Multiple sources for late-Holocene tsunamis at Discovery Bay, Washington State, USA. *Holocene* 15(1):60–73
- Wirth EA, Frankel AD. 2019. Impact of down-dip rupture limit and high-stress drop subevents on coseismic land-level change during Cascadia Megathrust earthquakes. *Bull. Seismol. Soc. Am.* 109(6):2187–97
- Wirth EA, Frankel AD, Marafi N, Vidale JE, Stephenson WJ. 2018. Broadband synthetic seismograms for magnitude 9 earthquakes on the Cascadia megathrust based on 3D simulations and stochastic synthetics, part 2: rupture parameters and variability. *Bull. Seismol. Soc. Am.* 108(5A):2370–88
- Witter RC, Jaffé B, Zhang Y, Priest G. 2012a. Reconstructing hydrodynamic flow parameters of the 1700 tsunami at Cannon Beach, Oregon, USA. *Nat. Hazards* 63(1):223–40
- Witter RC, Kelsey HM, Hemphill-Haley E. 2003. Great Cascadia earthquakes and tsunamis of the past 6700 years, Coquille River estuary, southern coastal Oregon. *GSA Bull.* 115(10):1289–306

- Witter RC, Zhang Y, Wang K, Goldfinger C, Priest GR, Allan JC. 2012b. Coseismic slip on the southern Cascadia megathrust implied by tsunami deposits in an Oregon lake and earthquake-triggered marine turbidites. *J. Geophys. Res.* 117(B10):B10303
- Witter RC, Zhang YJ, Wang K, Priest GR, Goldfinger C, et al. 2013. Simulated tsunami inundation for a range of Cascadia megathrust earthquake scenarios at Bandon, Oregon, USA. *Geosphere* 9(6):1783–803
- Wong FL, Grim MS. 2015. *Depth-to-basement, sediment-thickness, and bathymetry data for the deep-sea basins offshore of Washington, Oregon, and California*. Open File Rep. 2015-1118, US Geol. Surv., Seattle, WA
- Yamaguchi DK, Atwater BF, Bunker DE, Benson BE, Reid MS. 1997. Tree-ring dating the 1700 Cascadia earthquake. *Nature* 389(6654):922–23
- Ye L, Lay T, Kanamori H, Rivera L. 2016. Rupture characteristics of major and great ($M_w \geq 7.0$) megathrust earthquakes from 1990 to 2015: 2. Depth dependence. *J. Geophys. Res. Solid Earth* 121(2):845–63
- Yousefi M, Milne G, Li S, Wang K, Bartholet A. 2020. Constraining interseismic deformation of the Cascadia subduction zone: new insights from estimates of vertical land motion over different timescales. *J. Geophys. Res. Solid Earth* 125(3):e2019JB018248
- Zielke O. 2018. Earthquake recurrence and the resolution potential of tectono-geomorphic records. *Bull. Seismol. Soc. Am.* 108(3A):1399–413

Contents

Minoru Ozima: Autobiographical Notes <i>Minoru Ozima</i>	1
The Geodynamic Evolution of Iran <i>Robert J. Stern, Hadi Shafaii Moghadam, Mortaza Pirouz, and Walter Mooney</i>	9
Subduction-Driven Volatile Recycling: A Global Mass Balance <i>D.V. Bekaert, S.J. Turner, M.W. Broadley, J.D. Barnes, S.A. Halldórsson, J. Labidi, J. Wade, K.J. Walowski, and P.H. Barry</i>	37
Atmospheric Loss to Space and the History of Water on Mars <i>Bruce M. Jakosky</i>	71
Climate Risk Management <i>Klaus Keller, Casey Helgeson, and Vivek Srikrishnan</i>	95
Continental Drift with Deep Cratonic Roots <i>Masaki Yoshida and Kazunori Yoshizawa</i>	117
Contemporary Liquid Water on Mars? <i>James J. Wray</i>	141
Geologically Diverse Pluto and Charon: Implications for the Dwarf Planets of the Kuiper Belt <i>Jeffrey M. Moore and William B. McKinnon</i>	173
The Laurentian Great Lakes: A Biogeochemical Test Bed <i>Robert W. Sterner</i>	201
Clocks in Magmatic Rocks <i>Fidel Costa</i>	231
Hydration and Dehydration in Earth's Interior <i>Eiji Obtani</i>	253
Past Warmth and Its Impacts During the Holocene Thermal Maximum in Greenland <i>Yarrow Axford, Anne de Vernal, and Erich C. Osterberg</i>	279
Fiber-Optic Seismology <i>Nathaniel J. Lindsey and Eileen R. Martin</i>	309
Earth's First Redox Revolution <i>Chadlin M. Ostrander, Aleisha C. Johnson, and Ariel D. Anbar</i>	337

Toward an Integrative Geological and Geophysical View of Cascadia Subduction Zone Earthquakes <i>Maureen A.L. Walton, Lydia M. Staisch, Tina Dura, Jessie K. Pearl, Brian Sherrod, Joan Gomberg, Simon Engelbart, Anne Trébu, Janet Watt, Jon Perkins, Robert C. Witter, Noel Bartlow, Chris Goldfinger, Harvey Kelsey, Ann E. Morey, Valerie J. Sabakian, Harold Tobin, Kelin Wang, Ray Wells, and Erin Würth</i>	367
Recent Advances in Geochemical Paleo-Oxybarometers <i>Brian Kendall</i>	399
The Organic Isotopologue Frontier <i>Alexis Gilbert</i>	435
Olivine-Hosted Melt Inclusions: A Microscopic Perspective on a Complex Magmatic World <i>Paul J. Wallace, Terry Plank, Robert J. Bodnar, Glenn A. Gaetani, and Thomas Shea</i>	465
Architectural and Tectonic Control on the Segmentation of the Central American Volcanic Arc <i>Esteban Gazel, Kennet E. Flores, and Michael J. Carr</i>	495
Reactive Nitrogen Cycling in the Atmosphere and Ocean <i>Katy E. Altieri, Sarah E. Fawcett, and Meredith G. Hastings</i>	523
Submarine Landslides and Their Tsunami Hazard <i>David R. Tappin</i>	551
Titan's Interior Structure and Dynamics After the Cassini-Huygens Mission <i>Christophe Sotin, Klára Kalousová, and Gabriel Tobie</i>	579
Atmospheric CO ₂ over the Past 66 Million Years from Marine Archives <i>James W.B. Rae, Yi Ge Zhang, Xiaoqing Liu, Gavin L. Foster, Heather M. Stoll, and Ross D.M. Whiteford</i>	609
A 2020 Observational Perspective of Io <i>Imke de Pater, James T. Keane, Katherine de Kleer, and Ashley Gerard Davies</i>	643
An Atlas of Phanerozoic Paleogeographic Maps: The Seas Come In and the Seas Go Out <i>Christopher R. Scotese</i>	679

Errata

An online log of corrections to *Annual Review of Earth and Planetary Sciences* articles may be found at <http://www.annualreviews.org/errata/earth>

Related Articles

From the *Annual Review of Astronomy and Astrophysics*, Volume 58 (2020)

Observations of Protoplanetary Disk Structures

Sean M. Andrews

Astrochemistry During the Formation of Stars

Jes K. Jørgensen, Arnaud Belloche, and Robin T. Garrod

From the *Annual Review of Ecology, Evolution, and Systematics*, Volume 51 (2020)

Arthropod Origins: Integrating Paleontological and Molecular Evidence

Gregory D. Edgecombe

Origin and Evolution of the Turtle Body Plan

Tyler R. Lyson and Gabriel S. Bever

From the *Annual Review of Environment and Resources*, Volume 45 (2020)

Soil Microbiomes Under Climate Change and Implications for Carbon Cycling

Dan Naylor, Natalie Sadler, Arunima Bhattacharjee, Emily B. Graham,

Christopher R. Anderton, Ryan McClure, Mary Lipton,

Kirsten S. Hofmockel, and Janet K. Jansson

From the *Annual Review of Fluid Mechanics*, Volume 53 (2021)

Turbulence Processes Within Turbidity Currents

Mathew G. Wells and Robert M. Dorrell

Statistics of Extreme Events in Fluid Flows and Waves

Themistoklis P. Sapsis

Layering, Instabilities, and Mixing in Turbulent Stratified Flows

C.P. Caulfield

Mixing by Oceanic Lee Waves

Sonya Legg

From the *Annual Review of Marine Science*, Volume 13 (2021)

Right Place, Right Time: An Informal Memoir

Carl Wunsch

The Dissolution Rate of CaCO₃ in the Ocean

*Jess F. Adkins, John D. Naviaux, Adam V. Subbas, Sijia Dong,
and William M. Berelson*

The Complexity of Spills: The Fate of the *Deepwater Horizon* Oil

Uta Passow and Edward B. Overton

New Microbial Biodiversity in Marine Sediments

Brett J. Baker, Kathryn E. Appler, and Xianzhe Gong

Variations in Ocean Mixing from Seconds to Years

James N. Moum

Combining Modern and Paleoceanographic Perspectives on Ocean Heat Uptake

Geoffrey Gebbie

Historical Estimates of Surface Marine Temperatures

Elizabeth C. Kent and John J. Kennedy

Turbulence and Coral Reefs

Kristen A. Davis, Geno Pawlak, and Stephen G. Monismith

Amazon Sediment Transport and Accumulation Along the Continuum of Mixed
Fluvial and Marine Processes

*Charles A. Nittrouer, David J. DeMaster, Steven A. Kuehl, Alberto G. Figueiredo Jr.,
Richard W. Sternberg, L. Ercilio C. Faria, Odete M. Silveira, Mead A. Allison,
Gail C. Kineke, Andrea S. Ogston, Pedro W.M. Souza Filho, Nils E. Asp,
Daniel J. Nowacki, and Aaron T. Fricke*

The Origin of Modern Atolls: Challenging Darwin's Deeply Ingrained Theory

André W. Droxler and Stéphan J. Jorry

From the *Annual Review of Materials Research*, Volume 50 (2020)

Antisymmetry: Fundamentals and Applications

Hari Padmanabhan, Jason M. Munro, Ismaila Dabo, and Venkatraman Gopalan

Noble Metal Nanomaterials with Nontraditional Crystal Structures

Chaitali Sow, Suchithra P, Gangaiab Mettela, and Giridhar U. Kulkarni

High-Energy X-Ray Diffraction Microscopy in Materials Science

Joel V. Bernier, Robert M. Suter, Anthony D. Rollett, and Jonathan D. Almer

Frontiers in the Simulation of Dislocations

Nicolas Bertin, Ryan B. Sills, and Wei Cai

Grain Boundary Complexion Transitions

*Patrick R. Cantwell, Timofey Frolov, Timothy J. Rupert, Amanda R. Krause,
Christopher J. Marvel, Gregory S. Rohrer, Jeffrey M. Rickman,
and Martin P. Harmer*